AIMS Mathematics, 11(7): 21743–21780.
DOI: 10.3934/math.2026880
Received: 20 May 2026
Revised: 08 July 2026
Accepted: 10 July 2026
Published: 22 July 2026

https://www.aimspress.com/journal/Math

Research article

Generalized M-polynomial and graphical invariants of silicate cage networks with applications to property prediction

Zhang Yan[1], Muhammad Salman[2,*], Syed Shahzaib[2], Imran Khalid[3] and Hanen Karamti[4]

[1] School of Information Engineering, Anhui International Business Vocational College, Hefei, China
[2] Department of Mathematics, The Islamia University of Bahawalpur, Bahawalpur 63100, Pakistan
[3] Center for Advanced Studies in Pure and Applied Mathematics, Bahauddin Zakariya University, Multan 60800, Pakistan
[4] Department of Computer Sciences, College of Computer and Information Sciences, Princess Nourah bint Abdulrahman University, P.O. Box 84428, Riyadh 11671, Saudi Arabia

* **Correspondence:** Email: muhammad.salman@iub.edu.pk; Tel: +923326026668.

Abstract: This study introduces a generalized M-polynomial framework for the structural analysis of silicate cage molecular networks. From the molecular graph representation, several degree-based topological indices are derived, including Zagreb indices, the Randić index, the inverse Randić index, the symmetric division index, the harmonic index, the sum inverse index, and the augmented Zagreb index. The proposed formulation incorporates degree-weighted parameters, enabling a systematic characterization of structural complexity in terms of network parameters such as the number of layers and replicated units. Case-wise analysis for different structural configurations shows consistent trends in all indices, reflecting their sensitivity to molecular growth and connectivity. Overall, the results demonstrate that the proposed framework provides a unified and scalable approach for analyzing silicate cage networks. The obtained indices effectively capture structural variations and offer useful insights for graph-theoretical studies of complex molecular systems.

Keywords: silicate cage networks; generalized M-polynomial; topological indices; graph theory; molecular graph invariants
Mathematics Subject Classification: 05C10, 68R05, 68R10, 68T01

1. Introduction

In chemical graph theory, molecular structures are abstracted as mathematical graphs where atoms are represented by vertices and covalent bonds by edges. This representation provides a compact yet informative model that preserves the essential connectivity of a molecule while omitting complex

geometric and quantum mechanical details [1]. Such molecular graphs enable the derivation of topological indices that correlate structural patterns with physicochemical and biological properties [2].

Topological indices are numerical invariants that quantify molecular features such as branching, symmetry, and atomic environments. Since the introduction of the Hosoya index in 1971 [3] and the Zagreb indices by Gutman and Trinajstić in 1972 [4], degree-based indices have become central to quantitative structure-property relationship (QSPR) modeling [5]. Over time, new variants such as the general and inverse Randić, harmonic, symmetric division (SD), sum inverse (I), and augmented Zagreb (A) indices were proposed to enhance structural sensitivity and correlation performance [6]. These indices offer computational simplicity, requiring only two-dimensional (2D) connectivity information or simplified molecular input line entry system (SMILES) representations, and have been effectively used in high-throughput materials and drug discovery pipelines [7].

To unify the computation of such indices, Deutsch and Klavžar introduced the M-polynomial framework in 2015 [8]. The M-polynomial, defined as a bivariate generating function $M(G; x, y) = \sum_{uv \in E(G)} x^{d_u} y^{d_v}$, compactly encodes the degree distribution of a molecular graph. Through partial differentiation and integration, multiple degree-based indices can be derived from a single polynomial expression [9].

Silicate cage networks represent a particularly intriguing class of inorganic molecular architectures that lend themselves to topological modeling. Composed of corner-sharing $(TO_4)^{n-}$ tetrahedra, these frameworks exhibit periodic and symmetric connectivity patterns that can be elegantly represented through molecular graphs [10]. Found in materials such as zeolites, feldspars, and silsesquioxanes, silicate networks are valued for their high porosity, ion-exchange capacity, and catalytic activity [11]. Graph-theoretically, silicon and oxygen atoms can be modeled as degree-four and degree-two vertices, respectively, allowing structural regularity to be parameterized in terms of layer count (ν) and bond multiplicity (μ) [12].

The repetitive and modular nature of these frameworks makes them excellent candidates for M-polynomial-based generalization [8]. However, previous works have largely focused on analytical derivations without exploring predictive or data-driven correlations. To address this gap, the present work introduces a generalized M-polynomial that incorporates adjustable degree-weighting parameters, enhancing the sensitivity of topological indices toward structural variations in silicate cage networks. Unlike earlier M-polynomial studies that remained confined to symbolic formulations, this work establishes an explicit mathematical-computational bridge by coupling generalized topological indices with predictive analytics. This dual-layer contribution of analytical generalization and machine learning validation distinctly extends the applicability of graph theory in materials design.

Furthermore, these mathematically derived indices are integrated into a machine learning framework for property prediction. Machine learning, originating from the pioneering ideas of A. L. Samuel [13], has become a cornerstone of modern computational chemistry. Algorithms such as support vector machines (SVM), Random Forests, and deep neural networks have achieved exceptional accuracy in modeling complex, nonlinear chemical systems [14, 15]. In materials science, machine learning has demonstrated high predictive power for the mechanical, structural, and thermodynamic properties of silicate and oxide-based systems, achieving coefficients of determination $R^2 > 0.9$ across diverse datasets [16].

In this study, the structural properties of silicate cage networks are analyzed through degree-based topological indices derived from the generalized M-polynomial framework. The main objective is to

obtain exact analytical expressions for various indices and to examine how these descriptors vary with changes in the graph parameters. To further support the consistency of the derived results, regression-based validation is used as a supplementary tool to evaluate the trend behavior of these indices across different structural configurations. This integrated approach connects mathematical chemistry with data-driven analysis and provides a unified framework for interpreting the structural behavior of silicate cage networks. The use of regression analysis is not intended to predict unknown chemical properties; rather, it reinforces the reliability of the analytical formulas by confirming that they accurately reflect structural variations in the networks.

2. Silicate cage molecular network construction

In this work, we introduce two distinct ν-dimensional silicate frameworks, denoted as $SL_1(\nu)$ and $SL_2(\nu)$, which serve as the foundational motifs for higher-order network constructions. Each framework represents a silicate layer where the peripheral (boundary) atoms are chemically bonded to their mirror-image counterparts. Notably, each such mirrored atom is constrained to possess a coordination number (degree) of three, corresponding to the typical tetrahedral connectivity in silicate systems. This specific interconnection results in a bilayered topological structure, referred to here as a silicate cage network.

To generalize this structure, we extend the architecture to incorporate μ identical copies of the silicate unit SL_ν, arranged across ν benzene like planar layers. This yields a more intricate and repetitive structure termed the generalized silicate cage network, symbolically represented as $SLC_\mu(\nu)$. The underlying topology of this network reflects a hybrid design, coupling silicate tetrahedra with planar aromatic (benzene-like) conjugated units, enabling a robust three-dimensional (3D) molecular scaffold.

From a graph theoretical perspective, $V(SLC_\mu(\nu))$ denotes the set of atomic sites, while $E(SLC_\mu(\nu))$ represents the set of chemical bonds. The degree of each atom, d_u or d_v, corresponds to the number of adjacent bonded atoms, encapsulating the local bonding environment within the network. The structural complexity of $SLC_\mu(\nu)$ is examined under two chemically significant configurations.

(1) **Even-layered architecture** ($\nu \geq 2$, any $\mu \geq 2$): This represents the case where the number of layers is even, and multiple silicate units are stacked. The resulting structure exhibits high symmetry due to uniform interlayer connectivity, typically associated with stable silicate frameworks.
(2) **Odd-layered architecture** ($\nu \geq 3$, any $\mu \geq 3$): This involves an odd number of layers with three or more repeated silicate units. The resulting architecture is highly interconnected and complex, resembling zeolitic or nanocage structures with tunable pore geometries.

The analysis of silicate cage molecular networks is conducted under three structurally significant configurations: Fixed replication ($\mu = 2$), even layers (ν even), and odd layers (ν odd). These configurations were selected to capture fundamental variations in connectivity and symmetry. In the even-layer scenario, central vertices connect systematically to the corresponding vertices in adjacent layers, preserving structural symmetry. In contrast, the odd-layer scenario introduces a shift in central vertex connectivity, altering the degrees of certain vertices and edges. The fixed replication scenario isolates the effect of the number of units while maintaining a constant layer structure. This case-wise

analysis ensures that the derived topological indices comprehensively reflect variations in the network topology across different structural patterns.

The parameters ν and μ represent the number of silicate layers and the number of repeated silicate units, respectively, and their lower bounds are determined by structural feasibility rather than arbitrary choice. Specifically, $\nu \geq 2$ is imposed because a single layer cannot form a 3D cage; at least two interconnected layers are required to establish the full topology and interlayer bonding. Similarly, the minimum value of μ depends on the configuration: For the first configuration, $\mu = 2$ represents the smallest feasible cage and serves as a reference structure, while for the extended configurations, $\mu \geq 3$ ensures sufficient repetition to meaningfully analyze the network's growth, symmetry, and layer parity.

The three configurations represent successive stages of structural development rather than independent models. Analytical expressions for all degree-based topological indices exhibit a consistent dependence on ν and μ, with vertex and edge counts, as well as edge partitions, increasing systematically as either parameter grows. This behavior is consistently observed in both exact analytical formulas and regression-based validation.

Therefore, the selection of ν and μ depends on the study's structural objectives: Minimal configurations ($\mu = 2$, $\nu \geq 2$) are used to examine fundamental cage topology, while higher μ values allow an investigation of extended frameworks. The parity of ν is considered intentionally, as even- and odd-layered networks exhibit distinct boundary connectivity and edge partitions, yielding unique M-polynomials and closed-form expressions for topological indices. Separate analyses of these configurations are mathematically necessary and provide a comprehensive understanding of the structural evolution of generalized silicate cage networks.

These generalized cage networks are of particular interest for their potential applications in advanced materials, such as molecular sieves, ion-conductive frameworks, and nanoscale delivery systems. Furthermore, they offer a fertile ground for the exploration of topological indices, electronic delocalization, and coordination chemistry within hybrid inorganic-organic systems.

3. Methodology

The following definition of M-polynomial is the main tool used to evaluate the topological indices, listed in Table 1 , for $SLC_\mu(\nu)$.

For any graph $G = (V, E)$, the M-polynomial is defined as:

$$M(G; s, t) = g(s, t) = \sum_{n \leq p} m_{np}(G) s^n t^p, \tag{3.1}$$

where $m_{np}(G)$ represents number of bonds $uv \in E(G)$ such that $\{d_u(G), d_v(G)\} = \{n, p\}$ [17, 18]. The derivation of topological indices from the M-polynomial framework is performed analytically. For a network with V vertices and E edges, the evaluation of each degree-based index scales polynomially with the network's size. The computation involves systematic edge partitioning and summations over vertex degrees, ensuring tractable calculation even for larger networks.

Following the approach of Chen et al. [19], which analyzes computational complexity in graph-based regression frameworks, we note that the symbolic derivation of all nine topological indices can be completed efficiently, while regression-based validation scales linearly with the number of indices and observations. This demonstrates that the proposed method is computationally efficient

and scalable for all considered silicate cage network sizes. While methodologies from social network analysis and multiclass decision-making frameworks (see, e.g., [19]) inspire computational validation approaches, silicate cage networks represent fixed molecular connectivity with deterministic edge and vertex arrangements. Unlike social networks, which are dynamic and often probabilistic, our networks are entirely defined by the chemical structure. Consequently, the analyses of topological indices and regression-based validation focus purely on the molecular topology. References to advanced network methods provide context for complexity analyses and validation strategies but do not imply stochastic or social interactions in the studied molecular systems.

Let us define the topological index for a general molecular structure (graph) G as follows:

$$T(G) = \sum_{uv \in E(G)} f(d_u, d_v),$$

where $f(.,.)$ is a topological index function. This function is defined for underlined topological indices in Table 1, where $\lambda = d_u + d_v$ and $\eta = d_u \times d_v$.

Table 1. Topological index function of underlined topological indices.

Topological index	$T(G)$	$f(.,.)$	**Reference**
First Zagreb index	M_1	λ	[4, 20]
Second Zagreb index	M_2	η	[4, 21]
Modified second Zagreb index	M_2^m	$\frac{1}{\eta}$	[22]
General Randić index	R_α	η^α	[23]
Inverse Randić index	RR_α	$\frac{1}{\eta^\alpha}$	[24]
Symmetric division index	SD	$\frac{\lambda}{\eta}$	[25]
Harmonic index	H	$\frac{2}{\lambda}$	[26, 27]
Sum inverse index	I	$\frac{1}{\lambda}$	[28]
Augmented Zagreb index	A	$(\frac{\eta}{\lambda-2})^3$	[29]

In this article, we consider the honeycomb cage network $SLC_\mu(\nu)$ for $\nu \geq 2$ and $\mu \geq 2$ in the context of the above mentioned topological indices. An overview of our finding is depicted in Table 2, where

$$D_s f = s\frac{\partial g}{\partial s}, \quad D_t f = s\frac{\partial g}{\partial t}, \quad S_s f = \int_0^s \frac{g(r,t)}{r} dr,$$
$$S_t f = \int_0^t \frac{g(s,r)}{r} dr, \quad J(g(s,t)) = g(s,s), \quad Q_\alpha g = s^\alpha g.$$

All formulae given in Table 2 are calculated for $s = t = 1$ and $\alpha = -\frac{1}{2}$.

Table 2. Formulae of underline topological indices depending on the M-polynomial.

Topological indices	**Formulae based on** $g(s,t)$
First Zagreb index	$(D_s + D_t)g(s,t)$
Second Zagreb index	$(D_sD_t)g(s,t)$
Modified second Zagreb index	$(S_sS_t)g(s,t)$
General Randić index	$(D_s^\alpha D_t^\alpha)g(s,t)$
Inverse Randić index	$(S_s^\alpha S_t^\alpha)g(s,t)$
Symmetric division index	$(D_sS_t + S_sD_t)g(s,t)$
Harmonic index	$2S_sJD_sD_tg(s,t)$
Sum inverse index	$S_sJD_sD_tg(s,t)$
Augmented Zagreb index	$S_s^3Q_{-2}JD_s^3D_t^3g(s,t)$

4. The case when $\nu \geq 2$ is even and any $\mu \geq 2$

This section considers the case of an even number of layers $\nu \geq 2$ with multiple replicated units $\mu \geq 2$. The resulting silicate cage structure exhibits high symmetry and uniform interlayer connectivity. This symmetry leads to stable and predictable behavior of all degree-based topological indices. The graphical representation of $SLC_\mu(\nu)$ can be seen in Figure 1.

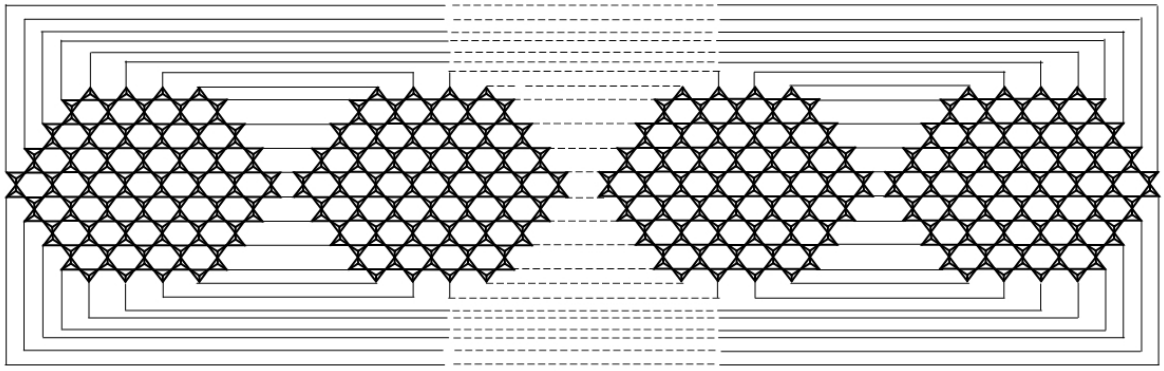

Figure 1. A generalized silicate cage network for an even number of layers and any $\mu \geq 3$ copies.

4.1. Mathematical modeling of indices

Note that $|V(SLC_\mu(\nu)| = 15\nu^2\mu + 3\nu\mu$ and $|E(SLC_\mu(\nu)| = 36\nu^2\mu + 3\nu\mu$. Table 3 presents the degree-based edge partitions for the minimal configuration ($\mu \geq 2$, $\nu \geq 2$). Each entry enumerates the number of edges connecting vertices of specified degrees. This table provides the foundational data for computing the topological indices in the subsequent analysis.

$$E_1(SLC_\mu(\nu)) = \{uv \in E_1(SLC_\mu(\nu)) : d_u = 3, d_v = 4\},$$
$$|E_1(SLC_\mu(\nu))| = 6\nu\mu,$$
$$E_2(SLC_\mu(\nu)) = \{uv \in E_2(SLC_\mu(\nu)) : d_u = 3, d_v = 6\},$$

$$|E_2(SLC_\mu(v))| = (18v^2 - 6v)\mu,$$
$$E_3(SLC_\mu(v)) = \{uv \in E_3(SLC_\mu(v)) : d_u = 4, d_v = 4\},$$
$$|E_3(SLC_\mu(v))| = 3v\mu,$$
$$E_4(SLC_\mu(v)) = \{uv \in E_4(SLC_\mu(v)) : d_u = 4, d_v = 6\},$$
$$|E_4(SLC_\mu(v))| = 12v\mu,$$
$$E_5(SLC_\mu(v)) = \{uv \in E_5(SLC_\mu(v)) : d_u = 6, d_v = 6\},$$
$$|E_5(SLC_\mu(v))| = (18v^2 - 12v)\mu.$$

By using the formula of M-polynomial, we get

$$M(SLC_\mu(v); s, t) = \sum_{n \le p} m_{np} s^n t^p = \sum_{3\le 4} m_{34} s^3 t^4 + \sum_{3\le 6} m_{36} s^3 t^6 + \sum_{4\le 4} m_{44} s^4 t^4 + \sum_{4\le 6} m_{46} s^4 t^6 + \sum_{6\le 6} m_{66} s^6 t^6$$
$$= |E_1(SLC_\mu(v))| + |E_2(SLC_\mu(v))| + |E_3(SLC_\mu(v))| + |E_4(SLC_\mu(v))| + |E_5(SLC_\mu(v))|,$$
$$M(SLC_\mu(v); s, t) = (6v\mu)s^3t^4 + (18v^2 - 6v)\mu s^3t^6 + (3v\mu)s^4t^4 + (12v\mu)s^4t^6 + (18v^2 - 12v)\mu s^6t^6. \quad (4.1)$$

By using formulae of Table 2 in Eq (4.1), we have

(1) $M_1(SLC_\mu(v)) = (D_s + D_t)g(s,t)|_{s=t=1} = 378(v^2\mu) - 12(v\mu)$;

(2) $M_2(SLC_\mu(v)) = D_sD_tg(s,t)|_{s=t=1} = 972(v^2\mu) - 132(v\mu)$;

(3) $M_2^m(SLC_\mu(v)) = (S_sS_t)g(s,t)|_{s=t=1} = \frac{3}{2}(v^2\mu) + \frac{25}{48}(v\mu)$;

(4) $R_\alpha(SLC_\mu(v)) = D_s^\alpha D_t^\alpha g(s,t)|_{s=t=1} = 12^\alpha(6v\mu) + 18^\alpha(18v^2 - 6v)\mu + 4^{2\alpha}(3v\mu) + 24^\alpha(12v\mu) + 6^{2\alpha}(18v^2 - 12v)\mu$;

(5) $RR_\alpha(SLC_\mu(v)) = S_s^\alpha S_t^\alpha g(s,t)|_{s=t=1} = 12^{-\alpha}(6v\mu) + 18^{-\alpha}(18v^2 - 6v)\mu + 4^{-2\alpha}(3v\mu) + 24^{-\alpha}(12v\mu) + 6^{-2\alpha}(18v^2 - 12v)\mu$;

(6) $SD(SLC_\mu(v)) = (D_sS_t + S_sD_t)g(s,t)|_{s=t=1} = 81(v^2\mu) + \frac{11}{2}(v\mu)$;

(7) $H(SLC_\mu(v)) = 2S_sJg(s,t)|_{s=1} = 7(v^2\mu) + \frac{643}{420}(v\mu)$;

(8) $I(SLC_\mu(v)) = S_sJD_sD_tg(s,t)|_{s=t=1} = 90(v^2\mu) - \frac{102}{35}(v\mu)$;

(9) $A(SLC_\mu(v)) = S_s^3Q_{-2}JD_s^3D_t^3g(s,t)|_{s=t=1} = 1145.8605(v^2\mu) - 198.0566(v\mu)$.

Table 3. Degree-based edge partition of $SLC_\mu(v)$.

(d_u, d_v)	$(3,4)$	$(3,6)$	$(4,4)$	$(4,6)$	$(6,6)$
Number of edges	$6v\mu$	$(18v^2 - 6v)\mu$	$3v\mu$	$12v\mu$	$(18v^2 - 12v)\mu$

4.2. Comparison of exact values for $\mu = 2$ and $v \ge 2$

The computed values of the underlined topological indices, derived using M-polynomial, are summarized in Table 4, where v and μ are assigned specific values and $\alpha = -\frac{1}{2}$. As demonstrated in Figure 2, the graph reflects the variations in topological indices based on the values of v and μ provided in Table 4.

Table 4. Computed values of topological indices for $SLC_{\mu}(\nu)$ with $\mu = 2$ and any $\nu \geq 2$.

ν	μ	M_1	M_2	M_2^m	R_α	RR_α	SD	H	I	A
2	2	2976	7248	14.08	64.01	670	1451.41	62.12	708.34	8374.66
3	2	6732	16704	30.12	139.47	1491	3283.31	135.19	1602.51	19437.15
4	2	12000	30048	52.17	243.90	2636	5852.69	236.25	2856.69	35083.08
5	2	18780	47280	80.21	377.31	4105	9159.54	365.31	4470.86	55312.46
6	2	27072	68400	114.25	539.68	5898	13203.86	522.37	6445.03	80125.28
7	2	36876	93408	154.29	731.02	8015	17985.65	707.43	8779.20	109521.54
8	2	48192	122304	200.33	951.34	10456	23504.91	920.50	11473.37	143501.24
9	2	61020	155088	252.38	1200.62	13221	29761.64	1161.56	14527.54	182064.38
10	2	75360	191760	310.42	1478.87	16310	36755.84	1430.62	17941.71	225210.97
11	2	91212	232320	374.46	1786.10	19723	44487.51	1727.68	21715.89	272941.00
12	2	108576	276768	444.50	2122.30	23460	52956.65	2052.74	25850.06	325254.47
13	2	127452	325104	520.54	2487.46	27521	62163.26	2405.80	30344.23	382151.38
14	2	147840	377328	602.58	2881.60	31906	72107.34	2786.87	35198.40	443631.73
15	2	169740	433440	690.62	3304.71	36615	82788.89	3195.93	40412.57	509695.53
16	2	193152	493440	784.67	3756.79	41648	94207.91	3632.99	45986.74	580342.76
17	2	218076	557328	884.71	4237.84	47005	106364.40	4098.05	51920.91	655573.44

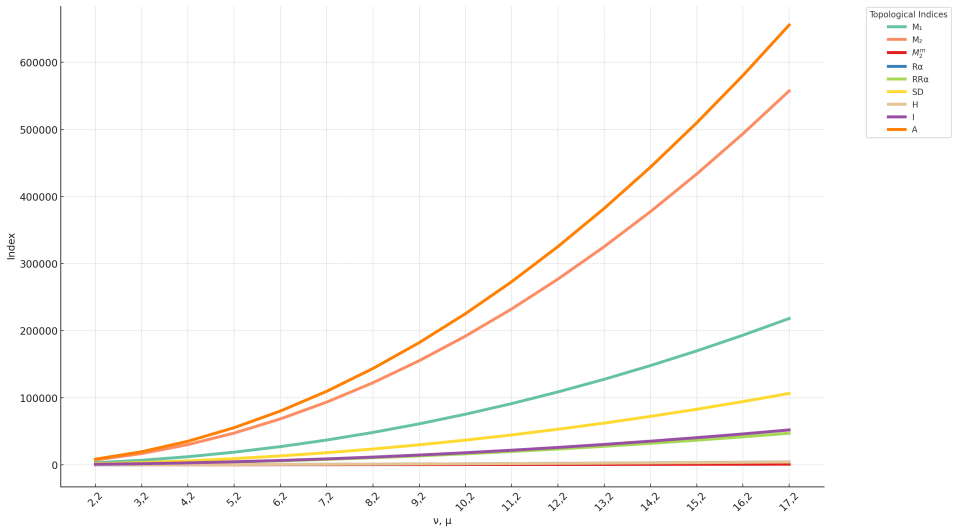

Figure 2. Comparison graph of topological indices for any $\nu \geq 2$ and $\mu = 2$.

4.2.1. Analytical and trend analysis for any $\nu \geq 2$ and $\mu = 2$

First Zagreb index: The variation in the the first Zagreb index with respect to the parameters ν and μ shows a consistent increasing trend. This indicates that the structural complexity of the silicate cage network increases with the growth of the network's size. The results presented in Table 5 and Figures 3 and 4 confirm that the computed analytical values follow a smooth and predictable pattern.

The observed behavior reflects the increasing connectivity and expansion of the molecular structure

$$M_1(SLC_\mu(\nu)) = 14340 \times \nu - 52164.$$

Second Zagreb index: The second Zagreb index exhibits a similar increasing trend with respect to ν. This indicates that degree-product-based structural contributions increase as the network grows. The results shown in Table 5 and Figures 5 and 6 confirm the smooth variation in the the computed analytical values, reflecting consistent structural behavior of the silicate cage network

$$M_2(SLC_\mu(\nu)) = 36672 \times \nu - 134136.$$

Modified second Zagreb index: The modified second Zagreb index shows a stable and regular growth pattern as the parameters increase. This indicates its sensitivity to local structural variations in the network. The results in Table 5 and Figures 7 and 8 support the analytical formulation and confirm consistent behavior across all parameter values

$$M_2^m(SLC_\mu(\nu)) = 58.04 \times \nu - 207.$$

General Randić index: The general Randić index increases steadily with respect to ν, reflecting its dependence on the branching and connectivity patterns of the network. The results presented in Table 5 and Figures 9 and 10 show a consistent variation in the computed analytical values, supporting the structural interpretation of the index

$$R_\alpha(SLC_\mu(\nu)) = 278.26 \times \nu - 999.49.$$

Inverse Randić index: The inverse Randić index shows a predictable increasing trend as the structural parameters increase. This reflects the dependence of the index on the connectivity structure of the graph. The results in Table 5 and Figures 11 and 12 confirm the smooth behavior of the analytical values

$$RR_\alpha(SLC_\mu(\nu)) = 3089 \times \nu - 11178.$$

Symmetric division index: The symmetric division index exhibits a steady increase with respect to ν, indicating strong dependence on structural connectivity. The results shown in Table 5 and Figures 13 and 14 confirm the consistency of the analytical expressions

$$SD(SLC_\mu(\nu)) = 6994.20 \times \nu - 25442.72.$$

Harmonic index: The harmonic index increases smoothly with respect to the structural parameters, reflecting its dependence on degree distribution within the network. The results in Table 5 and Figures 15 and 16 confirm the stable variation in the computed values

$$H(SLC_\mu(\nu)) = 269.06 \times \nu - 966.$$

Sum inverse index: The sum inverse index shows a consistent increasing trend as the network's size increases, indicating strong dependence on vertex connectivity. The results presented in Table 5 and Figures 17 and 18 support the analytical behavior of the index

$$I(SLC_\mu(\nu)) = 3414.17 \times \nu - 12420.$$

Augmented Zagreb index: The augmented Zagreb index exhibits a strong increasing trend with respect to ν, reflecting the higher-order structural sensitivity of the network. The results shown in Table 5 and Figures 19 and 20 confirm the correctness and stability of the analytical formulation

$$A(SLC_{\mu}(\nu)) = 43146.59 \times \nu - 158128.75.$$

Table 5. Predicted values of topological indices for $SLC_{\mu}(\nu)$ with $\mu = 2$ and any $\nu \geq 2$.

ν	μ	M_1	M_2	M_2^m	R_α	RR_α	SD	H	I	A
2	2	-23484	-60792	-90.92	-442.97	-5000	-11454.32	-427.88	-5591.66	-71835.57
3	2	-9144	-24120	-32.88	-164.71	-1911	-4460.12	-158.82	-2177.49	-28688.98
4	2	5196	12552	25.16	113.55	1178	2534.08	110.24	1236.68	14457.61
5	2	19536	49224	83.2	391.81	4267	9528.28	379.3	4650.85	57604.2
6	2	33876	85896	141.24	670.07	7356	16522.48	648.36	8065.02	100750.79
7	2	48216	122568	199.28	948.33	10445	23516.68	917.42	11479.19	143897.38
8	2	62556	159240	257.32	1226.59	13534	30510.88	1186.48	14893.36	187043.97
9	2	76896	195912	315.36	1504.85	16623	37505.08	1455.54	18307.53	230190.56
10	2	91236	232584	373.4	1783.11	19712	44499.28	1724.6	21721.7	273337.15
11	2	105576	269256	431.44	2061.37	22801	51493.48	1993.66	25135.87	316483.74
12	2	119916	305928	489.48	2339.63	25890	58487.68	2262.72	28550.04	359630.33
13	2	134256	342600	547.52	2617.89	28979	65481.88	2531.78	31964.21	402776.92
14	2	148596	379272	605.56	2896.15	32068	72476.08	2800.84	35378.38	445923.51
15	2	162936	415944	663.6	3174.41	35157	79470.28	3069.9	38792.55	489070.1
16	2	177276	452616	721.64	3452.67	38246	86464.48	3338.96	42206.72	532216.69
17	2	191616	489288	779.68	3730.93	41335	93458.68	3608.02	45620.89	575363.28

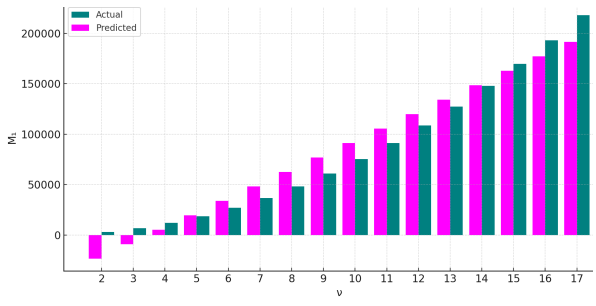

Figure 3. First Zagreb index vs ν.

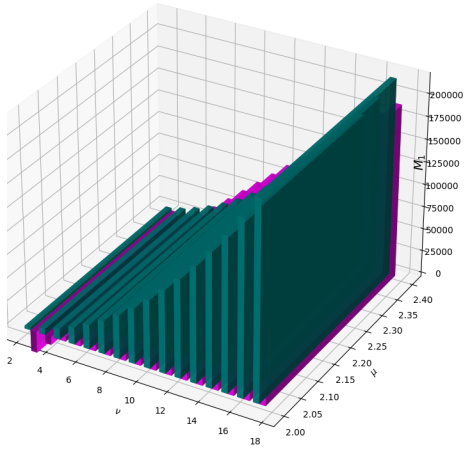

Figure 4. First Zagreb index vs ν and μ.

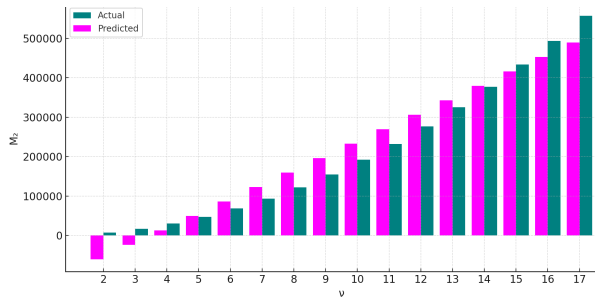

Figure 5. Second Zagreb index vs ν.

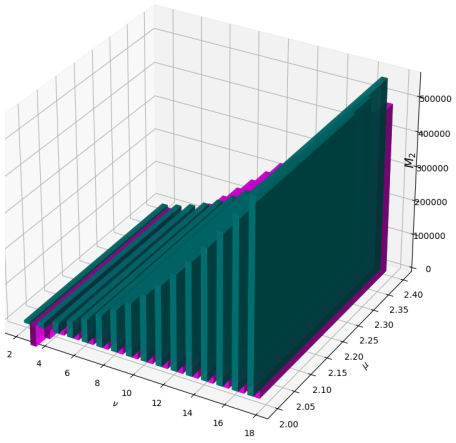

Figure 6. Second Zagreb index vs ν and μ.

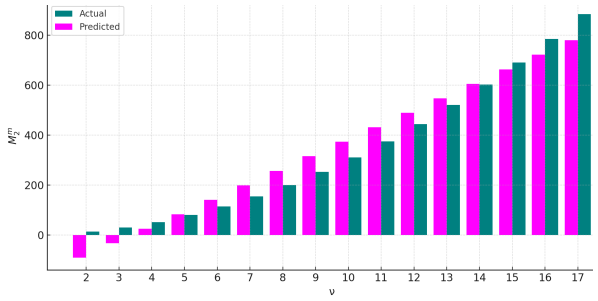

Figure 7. Modified second Zagreb index vs ν.

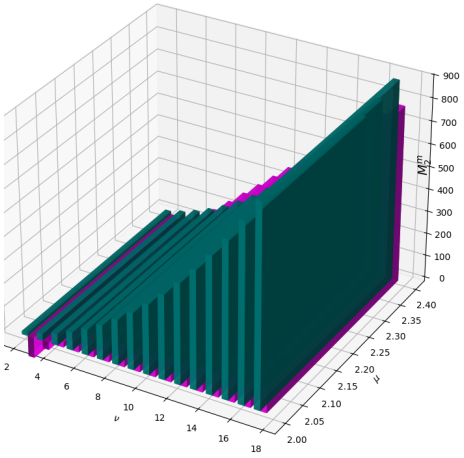

Figure 8. Modified second Zagreb index vs ν and μ.

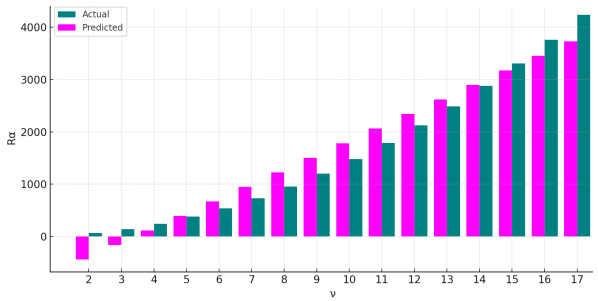

Figure 9. General Randić index vs ν.

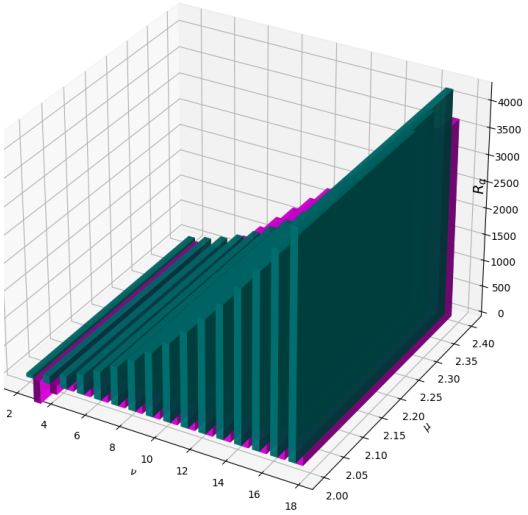

Figure 10. General Randić index vs ν and μ.

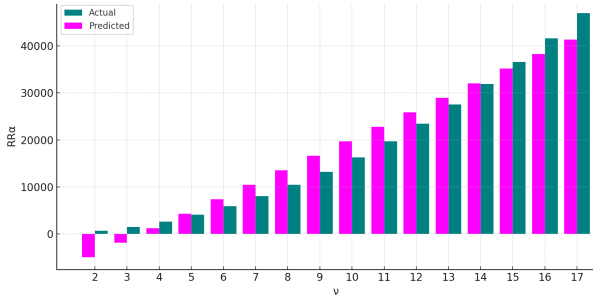

Figure 11. Inverse Randić index vs ν.

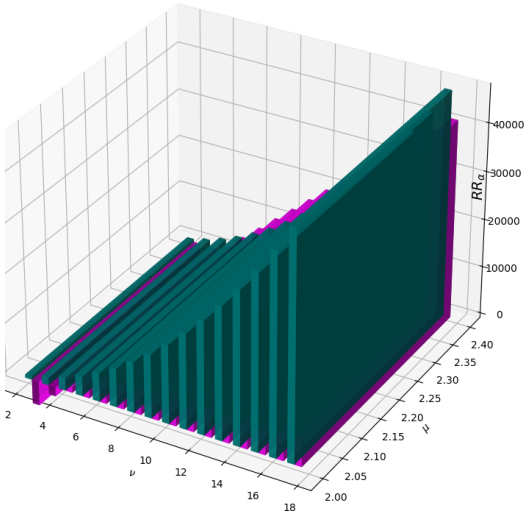

Figure 12. Inverse Randić index vs ν and μ.

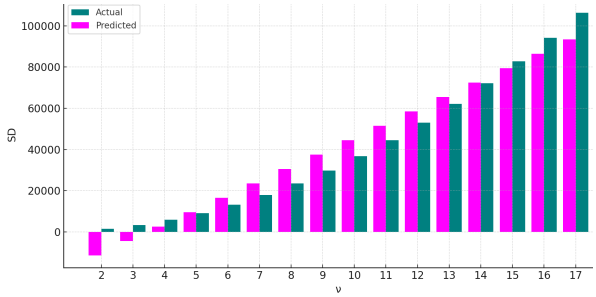

Figure 13. Symmetric division index vs ν.

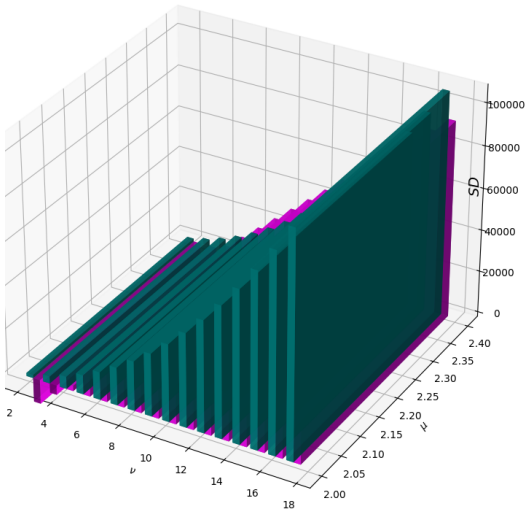

Figure 14. Symmetric division index vs ν and μ.

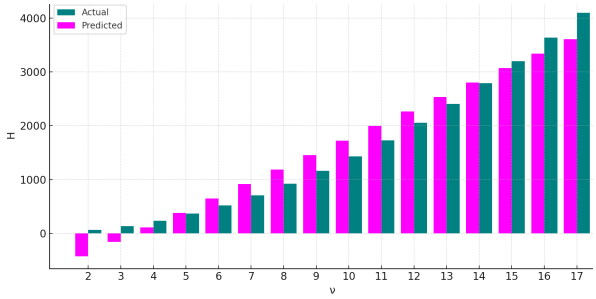

Figure 15. Harmonic index vs ν.

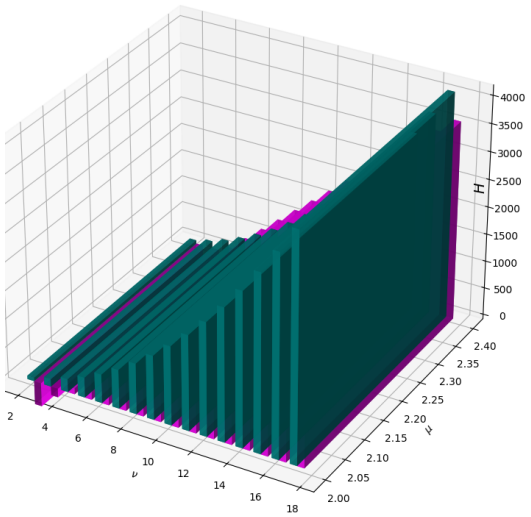

Figure 16. Harmonic index vs ν and μ.

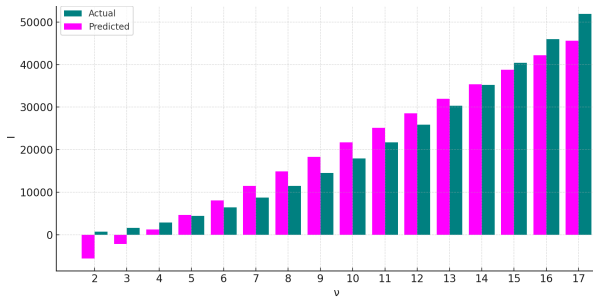

Figure 17. Sum inverse index vs ν.

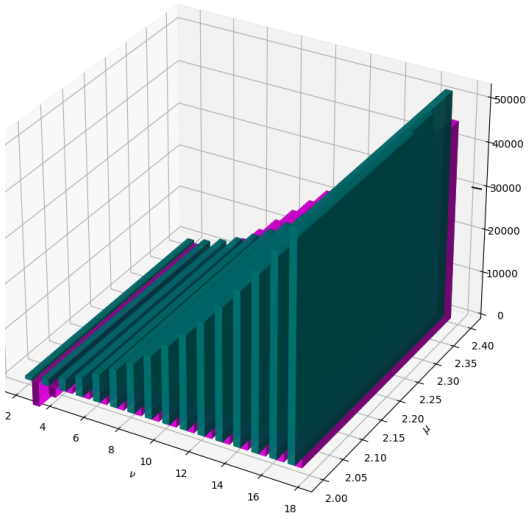

Figure 18. Sum inverse index vs ν and μ.

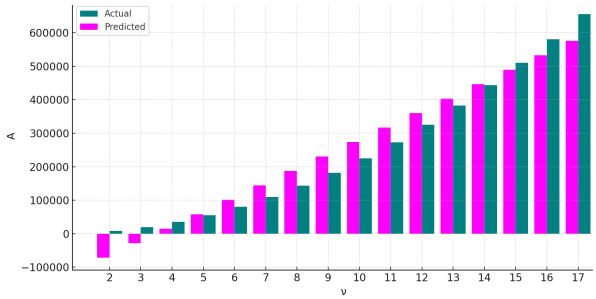

Figure 19. Augmented Zagreb index vs ν.

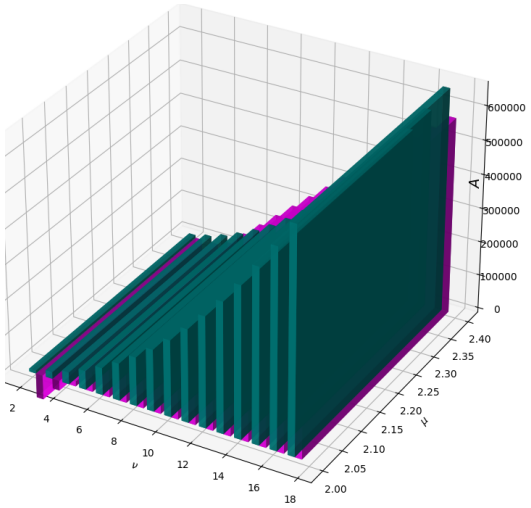

Figure 20. Augmented Zagreb index vs ν and μ.

4.2.2. Statistical analysis of all indices for $\mu = 2$

This section presents a statistical analysis of the computed values of nine key topological indices of silicate cage molecular networks, namely $M_1(S\,LC_\mu(\nu))$, $M_2(S\,LC_\mu(\nu))$, $M_2^m(S\,LC_\mu(\nu))$, $R_\alpha(S\,LC_\mu(\nu))$, $RR_\alpha(S\,LC_\mu(\nu))$, $S\,D(S\,LC_\mu(\nu))$, $H(S\,LC_\mu(\nu))$, $I(S\,LC_\mu(\nu))$, and $A(S\,LC_\mu(\nu))$, evaluated as functions of the number of layers ν and the number of units $\mu = 2$. These indices are visualized through both 2D and 3D graphical representations to better understand their structural behavior.

With respect to ν: In silicate cage networks, the variation in the topological indices as a function of ν provides important insights into the increasing structural complexity and connectivity of the molecular framework. As ν increases from 2 to 17, all considered topological indices, including M_1, M_2, M_2^m, R_α, RR_α, $S\,D$, H, I, and A, exhibit smooth and systematic growth patterns, typically following linear or polynomial trends. The first Zagreb index (M_1) and second Zagreb index (M_2) show a strong positive

correlation with ν, reflecting the increase in the degree sums and degree products as the network expands. The modified second Zagreb index (M_2^m) exhibits slightly non linear behavior, indicating sensitivity to local structural variations within the network. The harmonic index and Sum inverse index increase steadily, capturing the gradual rise in the diversity of connectivity. The Randić (R_α) and inverse Randić (RR_α) indices also show monotonic behavior, reflecting the growing branching complexity of the structure. The symmetric division index and augmented Zagreb index demonstrate relatively stronger growth, indicating their sensitivity to higher-order structural expansion and overall network density. These observed trends confirm that ν plays a fundamental role in governing the structural evolution and connectivity patterns of silicate cage molecular networks.

With respect to μ: Although the present study focuses on silicate cage networks with a fixed value $\mu = 2$, the parameter μ conceptually represents the number of replicated units and provides insight into interlayer connectivity effects. An increase in μ leads to higher bonding density and enhanced structural integration within the network. From a structural perspective, indices such as M_1 and M_2 are expected to increase with μ due to the direct contribution of additional edges to vertex degrees. Similarly, indices like M_2^m and RR_α are more sensitive to variations in inter-unit connectivity, reflecting changes in the local bonding configurations. Overall, increasing μ strengthens the structural framework and enhances the complexity of the silicate cage network.

4.3. Exact values comparison for $\mu \geq 3$ and an even $\nu \geq 2$

The underlined topological indices, obtained using the M-polynomial method, are presented in Table 6, where specific values of ν and μ are assigned, and α is set to $-\frac{1}{2}$. As shown in Figure 21, the graph illustrates the variations in these indices based on the ν and μ values listed in Table 6.

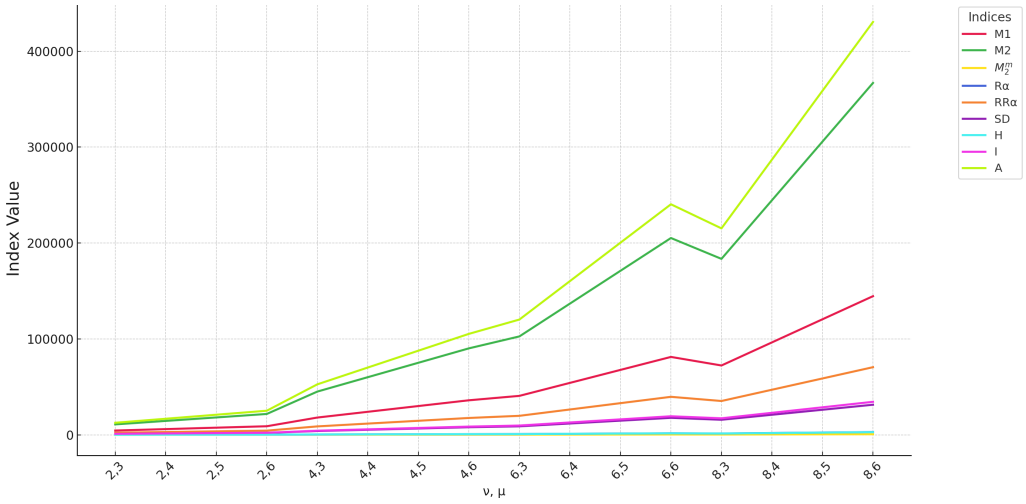

Figure 21. Comparison graph of topological indices for an even $\nu \geq 2$ and any $\mu \geq 3$.

Table 6. Computed values of topological indices for $SLC_\mu(\nu)$ with $\mu \geq 3$ and an even $\nu \geq 2$.

ν	μ	M_1	M_2	M_2^m	R_α	RR_α	SD	H	I	A
2	3	4464	10872	21.12	96.02	2177.11	1005	93	1062.51	12561.99
2	4	5952	14496	28.17	128.02	2902.81	1340	124	1416.69	16749.32
2	5	7440	18120	35.21	160.03	3628.52	1675	155	1770.86	20936.64
2	6	8928	21744	42.25	192.03	4354.22	2010	186	2125.03	25123.97
4	3	18000	45072	78.25	365.85	8779.04	3954	354	4285.03	52624.62
4	4	24000	60096	104.33	487.81	11705.39	5272	472	5713.37	70166.17
4	5	30000	75120	130.42	609.76	14631.73	6590	590	7141.71	87707.71
4	6	36000	90144	156.50	731.71	17558.08	7908	708	8570.06	105249.25
6	3	40608	102600	171.38	809.52	19805.79	8847	783	9667.54	120187.92
6	4	54144	136800	228.50	1079.36	26407.72	11796	1044	12890.06	160250.55
6	5	67680	171000	285.62	1349.20	33009.65	14745	1305	16112.57	200313.19
6	6	81216	205200	342.75	1619.03	39611.58	17694	1567	19335.09	240375.83
8	3	72288	183456	300.50	1427.00	35257.36	15684	1380	17210.06	215251.86
8	4	96384	244608	400.67	1902.67	47009.82	20912	1840	22946.74	287002.48
8	5	120480	305760	500.83	2378.34	58762.27	26140	2301	28683.43	358753.10
8	6	144576	366912	601.00	2854.01	70514.73	31368	2761	34420.11	430503.72

4.3.1. Structural analysis for an even number of layers and $\mu \geq 3$

First Zagreb index: The dependence of the first Zagreb index on the even number of layers $\nu \geq 2$ with replicated units $\mu \geq 3$ is presented in Table 7. Figures 22–24 provide graphical comparisons of the computed analytical values, illustrating the structural behavior of the silicate cage molecular network

$$M_1(SLC_\mu(\nu)) = 16956 \times \nu + 11280 \times \mu - 84780.$$

Second Zagreb index: The relationship between the second Zagreb index and the even number of layers $\nu \geq 2$ with replicated units $\mu \geq 3$ is detailed in Table 7. Figures 25–27 illustrate the variation in the computed analytical values, showing consistent structural trends

$$M_2(SLC_\mu(\nu)) = 43146 \times \nu + 28500 \times \mu - 215730.$$

Modified second Zagreb index: The correlation between the modified second Zagreb index and the parameters $\nu \geq 2$ and $\mu \geq 3$ is presented in Table 7. Figures 28–30 highlight the structural variation based on computed analytical values

$$M_2^m(SLC_\mu(\nu)) = 69.84 \times \nu + 47.60 \times \mu - 349.22.$$

General Randić index: The dependence of the general Randić index on $\nu \geq 2$ and $\mu \geq 3$ is summarized in Table 7. Figures 31–33 show the variation in the computed analytical values across the structural parameters

$$R_\alpha(SLC_\mu(\nu)) = 332.75 \times \nu + 224.87 \times \mu - 1663.73.$$

Inverse Randić index: The relationship between the inverse Randić index and the structural parameters is presented in Table 7. Figures 34–36 depict the variation in the computed analytical values

$$RR_{\alpha}(SLC_{\mu}(\nu)) = 8270.06 \times \nu + 5501.61 \times \mu - 41350.32.$$

Symmetric division index: The dependence of the symmetric division index on $\nu \geq 2$ and $\mu \geq 3$ is detailed in Table 7. Figures 37–39 present the structural variation in the computed analytical values

$$SD(SLC_{\mu}(\nu)) = 3669.75 \times \nu + 2457.50 \times \mu - 18348.75.$$

Harmonic index: The relationship between the harmonic index and the structural parameters is presented in Table 7. Figures 40–42 show the variation in the computed analytical values

$$H(SLC_{\mu}(\nu)) = 321.84 \times \nu + 217.68 \times \mu - 1609.79.$$

Sum inverse index: The dependence of the sum inverse index on $\nu \geq 2$ and $\mu \geq 3$ is summarized in Table 7. Figures 43–45 illustrate the structural variation in the computed analytical values

$$I(SLC_{\mu}(\nu)) = 4036.89 \times \nu + 2685.43 \times \mu - 20184.43.$$

Augmented Zagreb index: The correlation between the augmented Zagreb index and the structural parameters is presented in Table 7. Figures 46–48 illustrate the variation in the computed analytical values

$$A(SLC_{\mu}(\nu)) = 50672.47 \times \nu + 33385.53 \times \mu - 253362.34.$$

Table 7. Predicted values of topological indices for $SLC_{\mu}(\nu)$ with any $\mu \geq 3$ and an even $\nu \geq 2$.

ν	μ	M_1	M_2	M_2^m	R_{α}	RR_{α}	SD	H	I	A
2	3	-17028	-43938	-66.74	-323.62	-8305.37	-3636.75	-313.07	-4054.36	-51860.81
2	4	-5748	-15438	-19.14	-98.75	-2803.76	-1179.25	-95.39	-1368.93	-18475.28
2	5	5532	13062	28.46	126.12	2697.85	1278.25	122.29	1316.50	14910.25
2	6	16812	41562	76.06	350.99	8199.46	3735.75	339.97	4001.93	48295.78
4	3	16884	42354	72.94	341.88	8234.75	3702.75	330.61	4019.42	49484.13
4	4	28164	70854	120.54	566.75	13736.36	6160.25	548.29	6704.85	82869.66
4	5	39444	99354	168.14	791.62	19237.97	8617.75	765.97	9390.28	116255.19
4	6	50724	127854	215.74	1016.49	24739.58	11075.25	983.65	12075.71	149640.72
6	3	50796	128646	212.62	1007.38	24774.87	11042.25	974.29	12093.20	150829.07
6	4	62076	157146	260.22	1232.25	30276.48	13499.75	1191.97	14778.63	184214.60
6	5	73356	185646	307.82	1457.12	35778.09	15957.25	1409.65	17464.06	217600.13
6	6	84636	214146	355.42	1681.99	41279.70	18414.75	1627.33	20149.49	250985.66
8	3	84708	214938	352.30	1672.88	41314.99	18381.75	1617.97	20166.98	252174.01
8	4	95988	243438	399.90	1897.75	46816.60	20839.25	1835.65	22852.41	285559.54
8	5	107268	271938	447.50	2122.62	52318.21	23296.75	2053.33	25537.84	318945.07
8	6	118548	300438	495.10	2347.49	57819.82	25754.25	2271.01	28223.27	352330.60

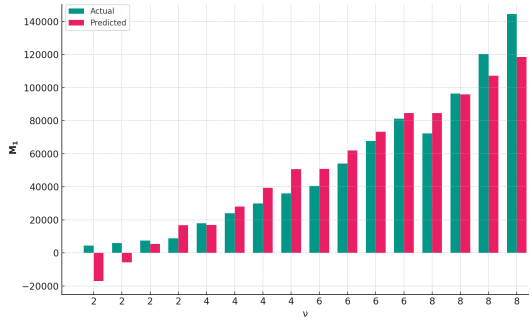

Figure 22. First Zagreb index vs ν.

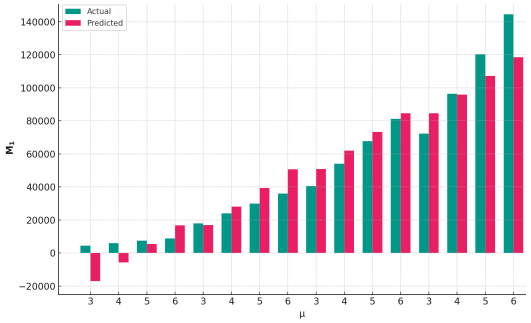

Figure 23. First Zagreb index vs μ.

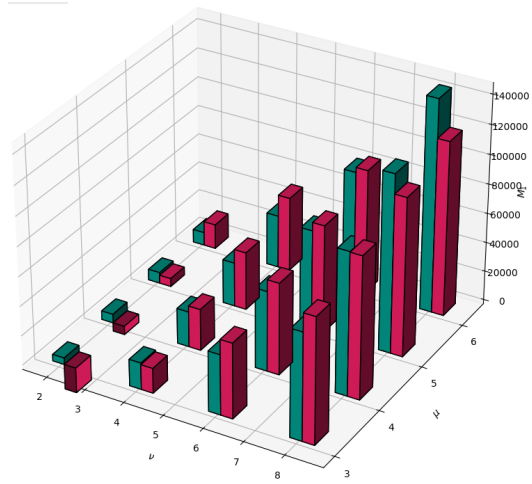

Figure 24. First Zagreb index vs ν and μ.

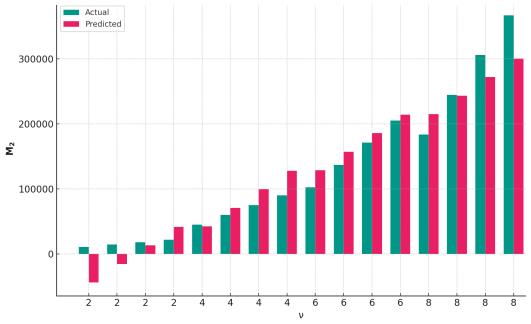

Figure 25. Second Zagreb index vs ν.

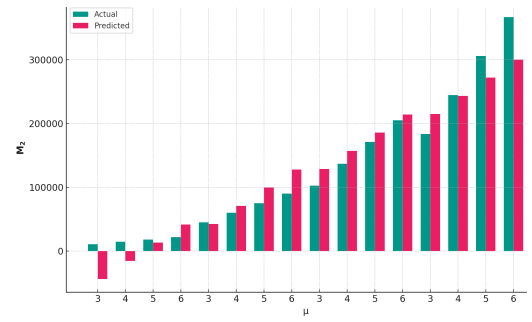

Figure 26. Second Zagreb index vs μ.

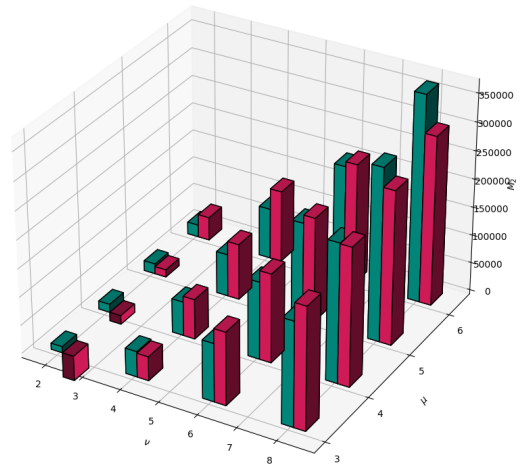

Figure 27. Second Zagreb index vs ν and μ.

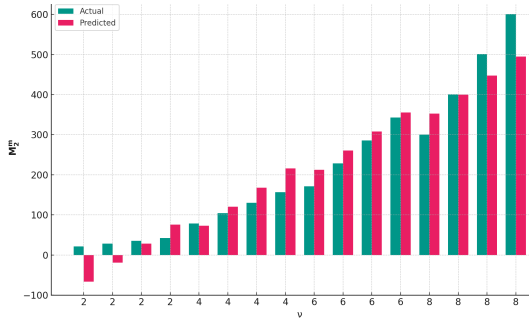

Figure 28. Modified second Zagreb index vs ν.

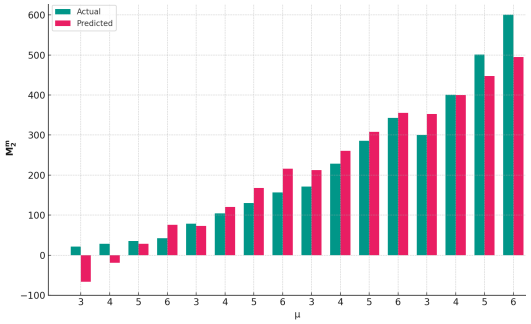

Figure 29. Modified second Zagreb index vs μ.

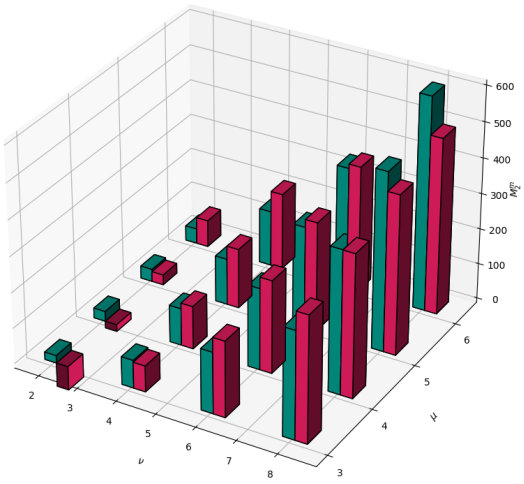

Figure 30. Modified second Zagreb index vs ν and μ.

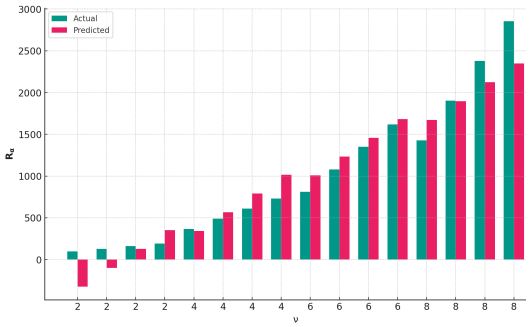

Figure 31. General Randić index vs ν.

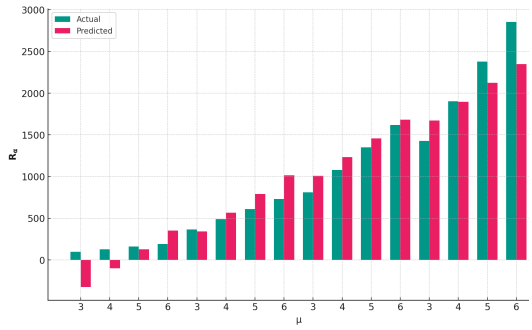

Figure 32. General Randić index vs μ.

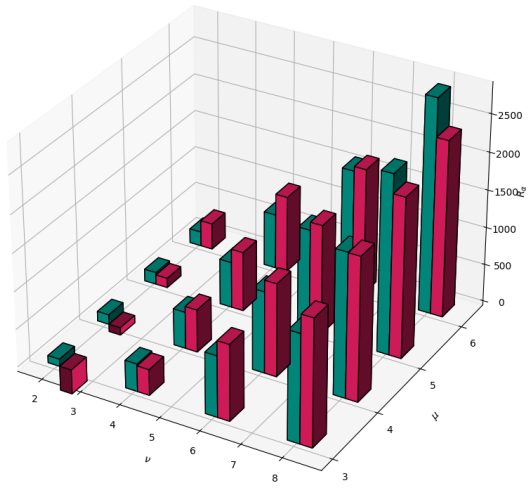

Figure 33. General Randić index vs ν and μ.

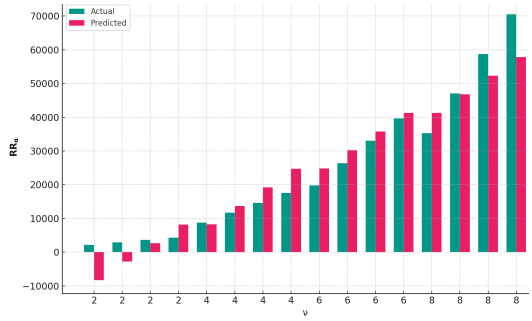

Figure 34. Inverse Randić index vs ν.

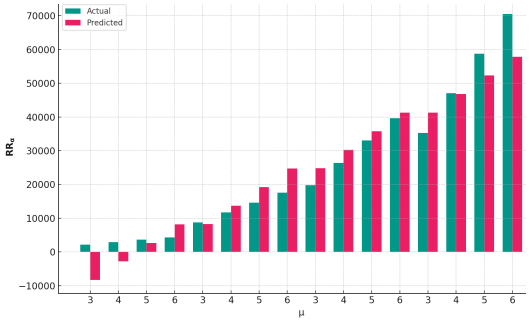

Figure 35. Inverse Randić index vs μ.

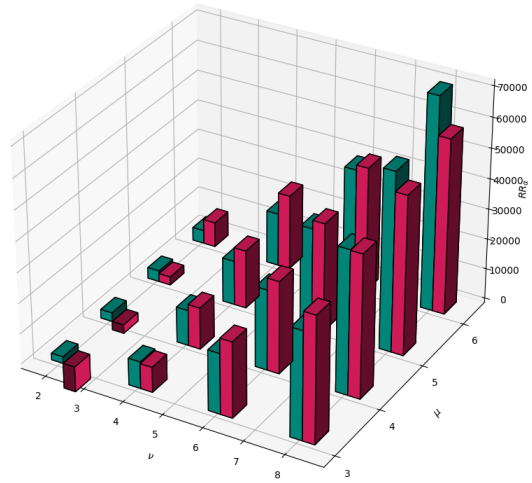

Figure 36. Inverse Randić index vs ν and μ.

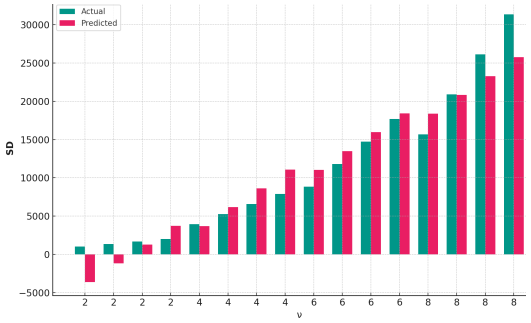

Figure 37. Symmetric division index vs ν.

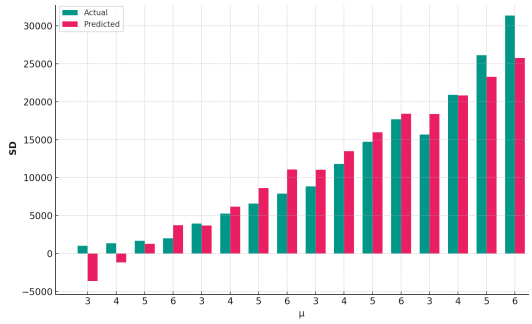

Figure 38. Symmetric division index vs μ.

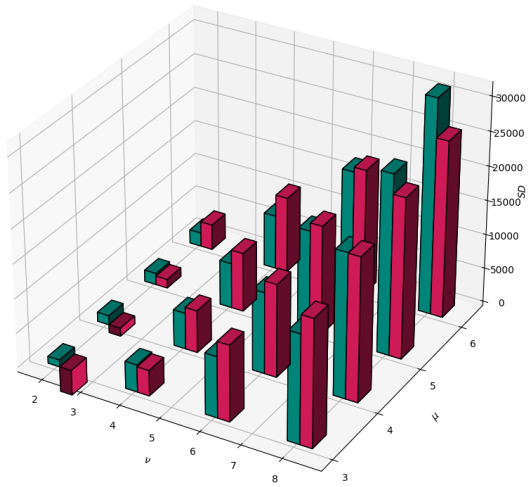

Figure 39. Symmetric division index vs ν and μ.

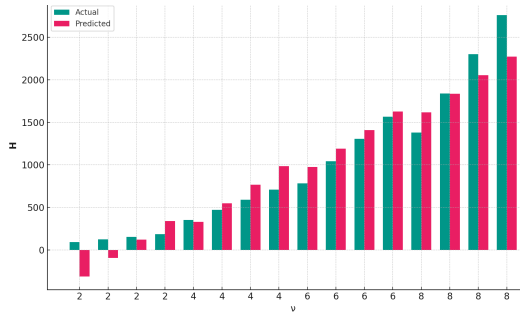

Figure 40. Harmonic index vs ν.

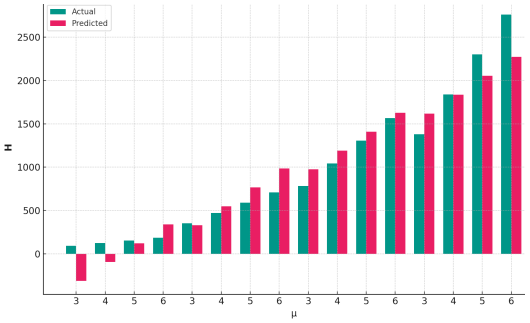

Figure 41. Harmonic index vs μ.

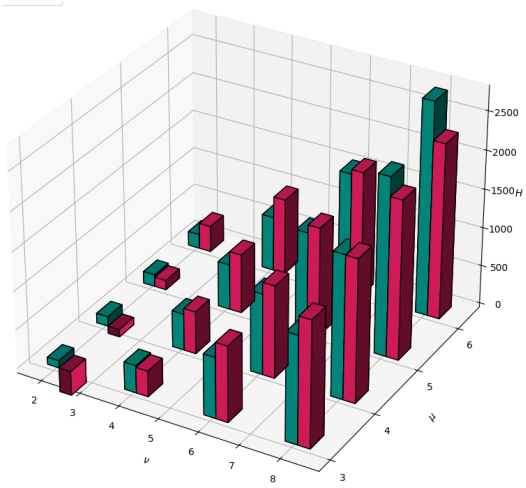

Figure 42. Harmonic index vs ν and μ.

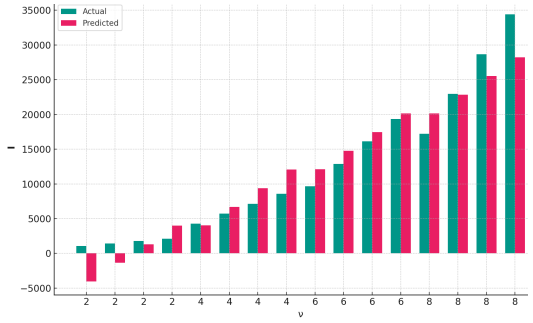

Figure 43. Sum inverse index vs ν.

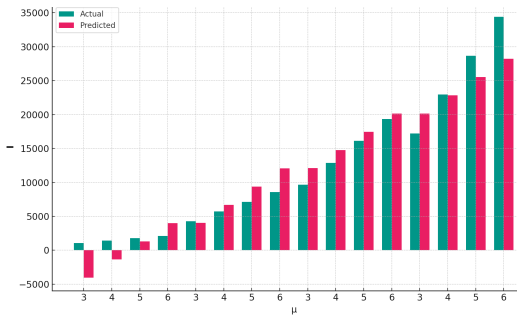

Figure 44. Sum inverse index vs μ.

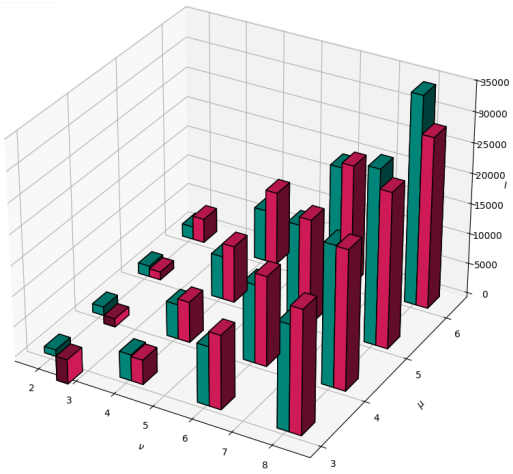

Figure 45. Sum inverse index vs ν and μ.

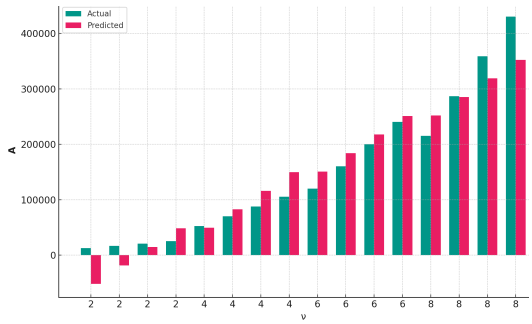

Figure 46. Augmented Zagreb index vs ν.

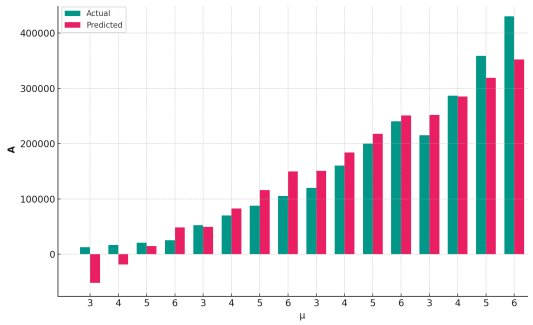

Figure 47. Augmented Zagreb index vs μ.

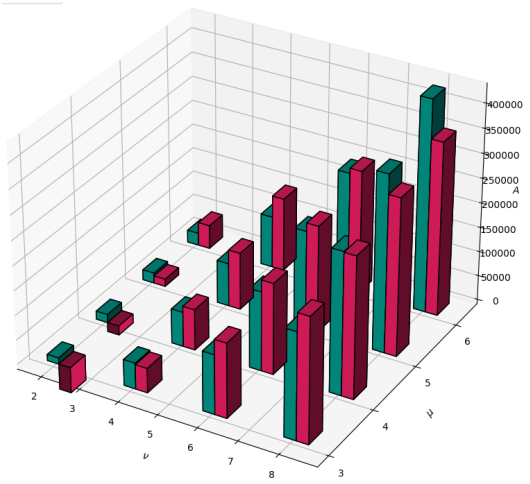

Figure 48. Augmented Zagreb index vs ν and μ.

4.3.2. Statistical analysis of all indices for even number of layers and $\mu \geq 3$

This section presents a statistical analysis of the computed values of nine topological indices of silicate cage molecular networks, specifically $M_1(SLC_\mu(\nu))$, $M_2(SLC_\mu(\nu))$, $M_2^m(SLC_\mu(\nu))$, $R_\alpha(SLC_\mu(\nu))$, $RR_\alpha(SLC_\mu(\nu))$, $SD(SLC_\mu(\nu))$, $H(SLC_\mu(\nu))$, $I(SLC_\mu(\nu))$, and $A(SLC_\mu(\nu))$, with respect to varying ν (the number of layers) and μ (the number of copies). The indices are visualized using both 2D and 3D graphical representations across the two parameters. A detailed discussion of the observed trends is provided below.

With respect to ν: As the number of layers ν increases from 2 to 8, all topological indices M_1, M_2, M_2^m, R_α, RR_α, SD, H, I, and A exhibit a consistent increasing trend. This behavior reflects the natural growth of the structural complexity, connectivity, and size of the silicate cage molecular network. Specifically, M_1 and M_2 show linear growth corresponding to increasing degree contributions. The modified second Zagreb index M_2^m reflects sensitivity to local structural variations. The indices R_α and RR_α increase steadily, indicating enhanced branching and connectivity paths within the network. The indices SD, H, I, and A also show increasing behavior, reflecting rising structural complexity and diversity in the molecular framework. Overall, the increase in all indices with respect to ν indicates that these indices

effectively capture size-dependent structural evolution in silicate cage networks, which is important in graph-theoretical chemistry and structural modeling applications.

With respect to μ: As the number of replicated units μ increases from 3 to 6, all indices show a strong positive dependence, indicating increased bonding density and enhanced structural integration in the network. In particular, M_2 and M_2^m increase significantly due to enhanced adjacency effects caused by higher connectivity. The indices R_α and RR_α also show stronger variation, reflecting increased branching complexity and connectivity paths. The indices SD, I, and A increase more rapidly compared with other indices, indicating higher sensitivity to structural expansion and interconnection effects. The harmonic index H shows relatively moderate variation, suggesting a balance between structural growth and the harmonic distribution of degrees. Overall, the behavior of all indices with respect to μ confirms its important role in controlling the connectivity and structural density of silicate cage molecular networks.

5. The case when $\nu \geq 3$ is odd and any $\mu \geq 3$

This section considers the case of an odd number of layers $\nu \geq 2$ with multiple replicated units $\mu \geq 3$. The resulting architecture is highly interconnected and complex, resembling zeolitic or nano cage structures with tunable pore geometries. The geometrical representation of $SLC_\mu(\nu)$ can be seen in Figure 49.

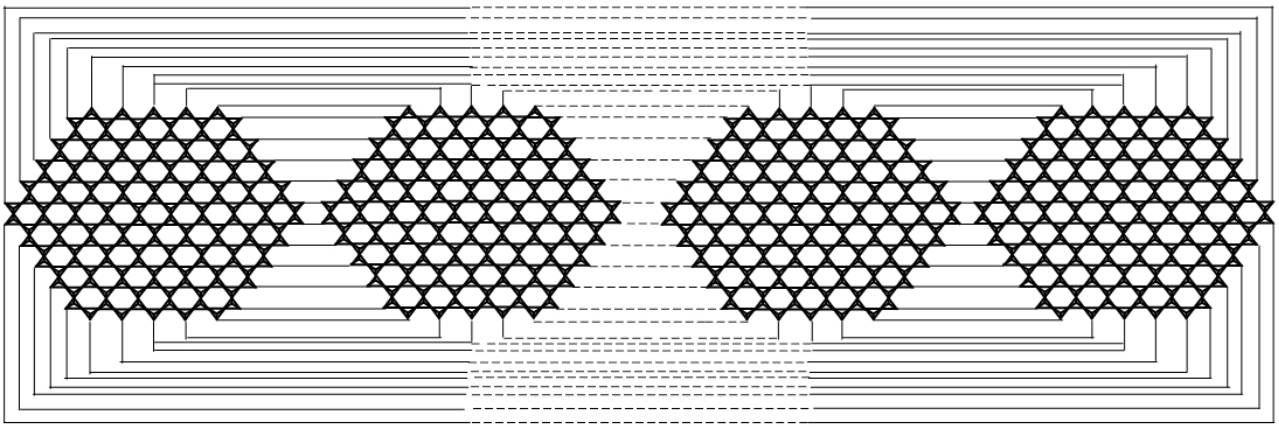

Figure 49. A generalized silicate cage molecular network for an odd number of layers $\nu \geq 3$ and any $\mu \geq 3$ copies.

5.1. Mathematical modeling of the indices

Note that $|V(SLC_\mu(\nu)| = 15\nu^2\mu + 3\nu\mu$ and $|E(SLC_\mu(\nu)| = 36\nu^2\mu + 3\nu\mu + \mu$. Table 9 presents the degree-based edge partitions for odd-layered configurations ($\nu \geq 3$, $\mu \geq 3$). Comparison with the minimal configuration demonstrates how increasing the number of layers and replicated units affects the vertex degrees and the distribution of edges, which, in turn, impacts the computed topological indices.

$$E_1(SLC_\mu(\nu)) = \{uv \in E_1(SLC_\mu(\nu)) : d_u = 3, d_v = 4\}, \qquad |E_1(SLC_\mu(\nu))| = (6\nu - 2)\mu,$$

$$E_2(SLC_\mu(v)) = \{uv \in E_2(SLC_\mu(v)) : d_u = 3, d_v = 5\}, \quad |E_2(SLC_\mu(v))| = 2\mu,$$
$$E_3(SLC_\mu(v)) = \{uv \in E_3(SLC_\mu(v)) : d_u = 3, d_v = 6\}, \quad |E_3(SLC_\mu(v))| = (18v^2 - 6v)\mu,$$
$$E_4(SLC_\mu(v)) = \{uv \in E_4(SLC_\mu(v)) : d_u = 4, d_v = 4\}, \quad |E_4(SLC_\mu(v))| = (3v - 1)\mu,$$
$$E_5(SLC_\mu(v)) = \{uv \in E_5(SLC_\mu(v)) : d_u = 4, d_v = 6\}, \quad |E_5(SLC_\mu(v))| = (12v - 4)\mu,$$
$$E_6(SLC_\mu(v)) = \{uv \in E_6(SLC_\mu(v)) : d_u = 5, d_v = 5\}, \quad |E_6(SLC_\mu(v))| = 2\mu,$$
$$E_7(SLC_\mu(v)) = \{uv \in E_7(SLC_\mu(v)) : d_u = 5, d_v = 6\}, \quad |E_7(SLC_\mu(v))| = 4\mu,$$
$$E_8(SLC_\mu(v)) = \{uv \in E_8(SLC_\mu(v)) : d_u = 6, d_v = 6\}, \quad |E_8(SLC_\mu(v))| = (18v^2 - 12v)\mu.$$

Table 8. Degree-based edge partition of $SLC_\mu(v)$.

(d_u, d_v)	$(3,4)$	$(3,5)$	$(3,6)$	$(4,4)$	$(4,6)$	$(5,5)$	$(5,6)$	$(6,6)$
No. of bonds	$(6v-2)\mu$	2μ	$(18v^2-6v)\mu$	$(3v-1)\mu$	$(12v-4)\mu$	2μ	4μ	$(18v^2-12v)\mu$

By using the formula of M-polynomials, we get

$$\begin{aligned}
M(SLC_\mu(v); s, t) &= \sum_{n\le p} m_{np} s^n t^p \\
&= \sum_{3\le 4} m_{34} s^3 t^4 + \sum_{3\le 5} m_{35} s^3 t^5 + \sum_{3\le 6} m_{36} s^3 t^6 + \sum_{4\le 4} m_{44} s^4 t^4 + \sum_{4\le 6} m_{46} s^4 t^6 \\
&\quad + \sum_{5\le 5} m_{55} s^5 t^5 + \sum_{5\le 6} m_{56} s^5 t^6 + \sum_{6\le 6} m_{66} s^6 t^6 \\
&= |E_1(SLC_\mu(v))| + |E_2(SLC_\mu(v))| + |E_3(SLC_\mu(v))| + |E_4(SLC_\mu(v))| \\
&\quad + |E_5(SLC_\mu(v))| + |E_6(SLC_\mu(v))| + |E_7(SLC_\mu(v))| + |E_8(SLC_\mu(v))|, \\
M(SLC_\mu(v); s, t) &= (6v-2)\mu s^3 t^4 + 2\mu s^3 t^5 + (18v^2 - 6v)\mu s^3 t^6 \\
&\quad + (3v-1)\mu s^4 t^4 + (12v-4)\mu s^4 t^6 + 2\mu s^5 t^5 \\
&\quad + 4\mu s^5 t^6 + (18v^2 - 12v)\mu s^6 t^6. \qquad (5.1)
\end{aligned}$$

By using the formulae of Table 2 in Eq (5.1), we have

(1) $M_1(SLC_\mu(v)) = (D_s + D_t)g(s,t)|_{s=t=1} = 378(v^2\mu) - 12(v\mu) + 18(\mu)$;

(2) $M_2(SLC_\mu(v)) = D_s D_t g(s,t)|_{s=t=1} = 972(v^2\mu) - 132(v\mu) + 64(\mu)$;

(3) $M_2^m(SLC_\mu(v)) = (S_s S_t)g(s,t)|_{s=t=1} = \frac{3}{2}(v^2\mu) + \frac{25}{48}(v\mu) - \frac{59}{1200}(\mu)$;

(4) $R_\alpha(SLC_\mu(v)) = D_s^\alpha D_t^\alpha g(s,t)|_{s=t=1} = 12^\alpha(6v-2)\mu + 15^\alpha(2\mu) + 18^\alpha(18v^2 - 6v)\mu + 4^{2\alpha}(3v-1)\mu + 24^\alpha(12v-4)\mu + 5^{2\alpha}(2\mu) + 30^\alpha(4\mu) + 6^{2\alpha}(18v^2 - 12v)\mu$;

(5) $RR_\alpha(SLC_\mu(v)) = S_s^\alpha S_t^\alpha g(s,t)|_{s=t=1} = 12^{-\alpha}(6v-2)\mu + 15^{-\alpha}(2\mu) + 18^{-\alpha}(18v^2 - 6v)\mu + 4^{-2\alpha}(3v-1)\mu + 24^{-\alpha}(12v-4)\mu + 5^{-2\alpha}(2\mu) + 30^{-\alpha}(4\mu) + 6^{-2\alpha}(18v^2 - 12v)\mu$;

(6) $SD(SLC_\mu(v)) = (D_s S_t + S_s D_t)g(s,t)|_{s=t=1} = 81(v^2\mu) + \frac{11}{2}(v\mu) + \frac{11}{6}(\mu)$;

(7) $H(SLC_\mu(v)) = 2S_s J g(s,t)|_{s=1} = 7(v^2\mu) + \frac{643}{420}(v\mu) + \frac{9}{1540}(\mu)$;

(8) $I(SLC_\mu(v)) = S_s J D_s D_t g(s,t)|_{s=t=1} = 90(v^2\mu) - \frac{102}{35}(v\mu) + \frac{7131}{1540}(\mu)$;

(9) $A(SLC_\mu(v)) = S_s^3 Q_{-2} J D_s^3 D_t^3 g(s,t)|_{s=t=1} = 1145.8605(v^2\mu) - 198.0566(v\mu) - 24.7872(\mu)$.

5.2. *Exact values comparison for when $\nu \geq 3$ is odd and any $\mu \geq 3$*

The underlined topological indices, calculated using the M-polynomial approach, are detailed in Table 9, with designated values for ν and μ, and α fixed at $-\frac{1}{2}$. Figure 50 visually represents the changes in these indices, reflecting the corresponding ν and μ values provided in Table 9.

Table 9. Computed values of topological indices for $HCC_{\mu}(\nu)$ with $\mu \geq 3$ and an odd $\nu \geq 3$.

ν	μ	M_1	M_2	M_2^m	R_α	RR_α	SD	H	I	A
3	3	10152	25248	44.30	209.22	4952.36	2242.00	202.80	2417.66	29081.36
3	4	13536	33664	59.07	278.95	6603.15	2989.33	270.39	3223.55	38775.15
3	5	16920	42080	73.84	348.69	8253.94	3736.67	337.99	4029.44	48468.94
3	6	20304	50496	88.60	418.43	9904.73	4484.00	405.59	4835.33	58162.72
5	3	28224	71112	119.43	565.97	13766.70	6163.00	547.98	6720.18	82894.33
5	4	37632	94816	159.24	754.62	18355.61	8217.33	730.64	8960.24	110525.77
5	5	47040	118520	199.05	943.28	22944.51	10271.67	913.30	11200.30	138157.21
5	6	56448	142224	238.86	1131.93	27533.41	12326.00	1095.96	13440.35	165788.65
7	3	55368	140304	230.55	1096.54	27005.87	12028.00	1061.17	13182.69	164207.94
7	4	73824	187072	307.40	1462.05	36007.82	16037.33	1414.89	17576.92	218943.92
7	5	92280	233840	384.25	1827.57	45009.78	20046.67	1768.61	21971.15	273679.91
7	6	110736	280608	461.10	2193.08	54011.73	24056.00	2122.34	26365.38	328415.89
9	3	91584	232824	377.68	1800.94	44669.85	19837.00	1742.35	21805.21	273022.21
9	4	122112	310432	503.57	2401.25	59559.80	26449.33	2323.14	29073.61	364029.62
9	5	152640	388040	629.46	3001.56	74449.75	33061.67	2903.92	36342.01	455037.02
9	6	183168	465648	755.36	3601.88	89339.70	39674.00	3484.71	43610.41	546044.42

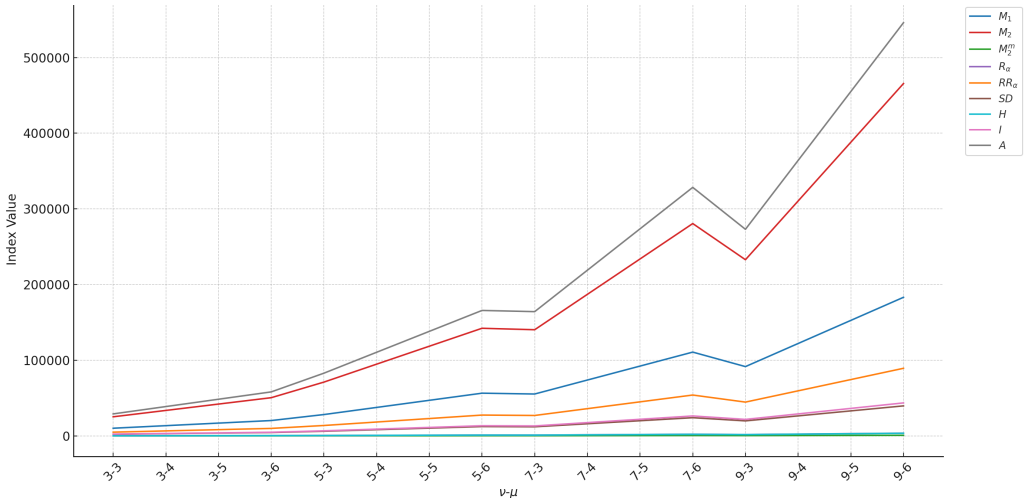

Figure 50. Comparison graph of topological indices for $\nu \geq 3$ and $\mu \geq 3$.

5.3. Topological behavior for any odd number of layers and $\mu \geq 3$

First Zagreb index: The dependence of the first Zagreb index on the odd number of layers $\nu \geq 3$ and the number of replicated units $\mu \geq 3$ is summarized in Table 10. Figures 51–53 present a graphical representation of the computed analytical values, illustrating the structural behavior of the extended silicate cage molecular network

$$M_1(S\,LC_\mu(\nu)) = 20358 \times \nu + 15444 \times \mu - 122148.$$

Second Zagreb index: The second Zagreb index shows a consistent variation with respect to ν and μ, as presented in Table 10. Figures 54–56 illustrate the structural trends of the computed analytical values

$$M_2(S\,LC_\mu(\nu)) = 51894 \times \nu + 39124 \times \mu - 311364.$$

Modified second Zagreb index: The modified second Zagreb index exhibits stable dependence on ν and μ, as shown in Table 10. Figures 57–59 present the variation in the computed analytical values

$$M_2^m(S\,LLC_\mu(\nu)) = 83.34 \times \nu + 64.33 \times \mu - 500.06.$$

General Randić index: The general Randić index behavior is summarized in Table 10. Figures 60–62 show the variation in the computed analytical values

$$R_\alpha(S\,LC_\mu(\nu)) = 397.93 \times \nu + 306.05 \times \mu - 2387.58.$$

Inverse Randić index: The inverse Randić index variation is presented in Table 10. Figures 63–65 illustrate the behavior of the computed analytical values

$$RR_\alpha(S\,LC_\mu(\nu)) = 9929.37 \times \nu + 7532.90 \times \mu - 59576.23.$$

Symmetric division index: The symmetric division index shows steady variation with respect to structural parameters, as shown in Table 10. Figures 66–68 present the computed analytical trends

$$S\,D(S\,LC_\mu(\nu)) = 4398.75 \times \nu + 3355.83 \times \mu - 26392.50.$$

Harmonic index: The harmonic index behavior is summarized in Table 10. Figures 69–71 show variation in the computed analytical values

$$H(S\,LC_\mu(\nu)) = 384.89 \times \nu + 296.19 \times \mu - 2309.34.$$

Sum inverse index: The sum inverse index variation is presented in Table 10. Figures 72–74 illustrate the computed analytical trends

$$I(S\,LC_\mu(\nu)) = 4846.89 \times \nu + 3677.14 \times \mu - 29081.31.$$

Augmented Zagreb index: The augmented Zagreb index behavior is shown in Table 10. Figures 75–77 present the computed analytical variation

$$A(S\,LC_\mu(\nu)) = 60985.21 \times \nu + 45767.15 \times \mu - 365911.27.$$

Table 10. Predicted values of topological indices for $SLC_{\mu}(\nu)$ with any $\mu \geq 3$ and any $\nu \geq 3$.

ν	μ	M_1	M_2	M_2^m	R_α	RR_α	SD	H	I	A
3	3	-14742	-38310	-57.05	-275.64	-7189.42	-3128.76	-266.1	-3509.22	-45654.19
3	4	702	814	7.28	30.41	343.48	227.07	30.09	167.92	112.96
3	5	16146	39938	71.61	336.46	7876.38	3582.9	326.28	3845.06	45880.11
3	6	31590	79062	135.94	642.51	15409.28	6938.73	622.47	7522.2	91647.26
5	3	25974	65478	109.63	520.22	12669.32	5668.74	503.68	6184.56	76316.23
5	4	41418	104602	173.96	826.27	20202.22	9024.57	799.87	9861.7	122083.38
5	5	56862	143726	238.29	1132.32	27735.12	12380.4	1096.06	13538.84	167850.53
5	6	72306	182850	302.62	1438.37	35268.02	15736.23	1392.25	17215.98	213617.68
7	3	66690	169266	276.31	1316.08	32528.06	14466.24	1273.46	15878.34	198286.65
7	4	82134	208390	340.64	1622.13	40060.96	17822.07	1569.65	19555.48	244053.8
7	5	97578	247514	404.97	1928.18	47593.86	21177.9	1865.84	23232.62	289820.95
7	6	113022	286638	469.3	2234.23	55126.76	24533.73	2162.03	26909.76	335588.1
9	3	107406	273054	442.99	2111.94	52386.8	23263.74	2043.24	25572.12	320257.07
9	4	122850	312178	507.32	2417.99	59919.7	26619.57	2339.43	29249.26	366024.22
9	5	138294	351302	571.65	2724.04	67452.6	29975.4	2635.62	32926.4	411791.37
9	6	153738	390426	635.98	3030.09	74985.5	33331.23	2931.81	36603.54	457558.52

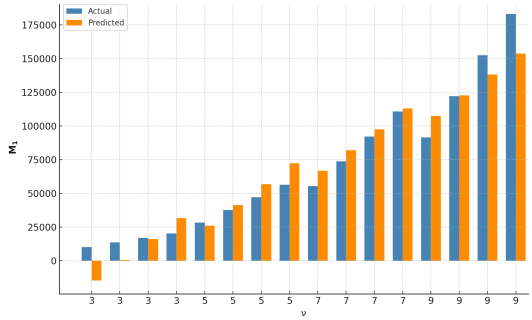

Figure 51. First Zagreb index vs ν.

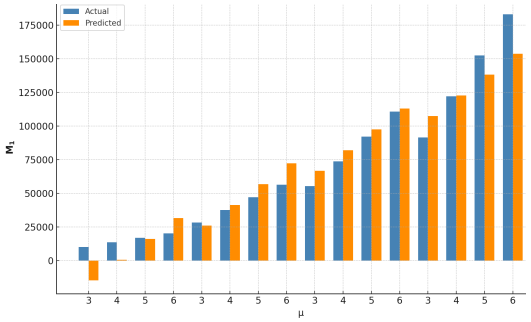

Figure 52. First Zagreb index vs μ.

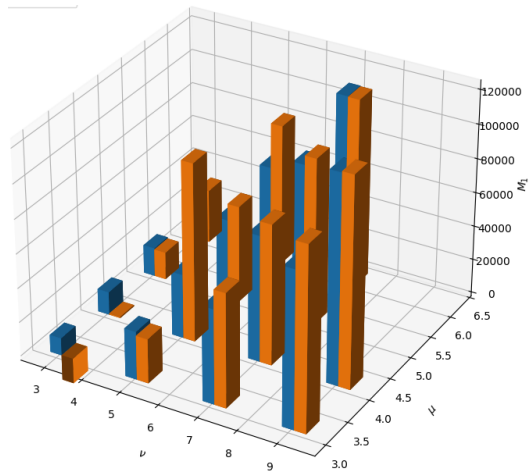

Figure 53. First Zagreb index vs ν and μ.

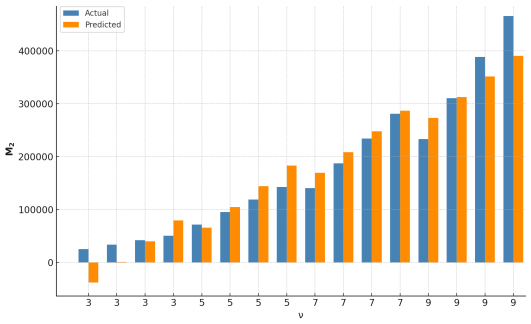

Figure 54. Second Zagreb index vs ν.

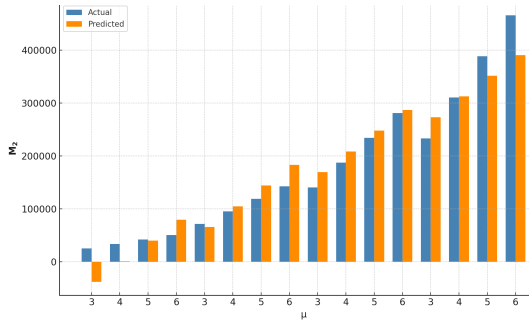

Figure 55. Second Zagreb index vs μ.

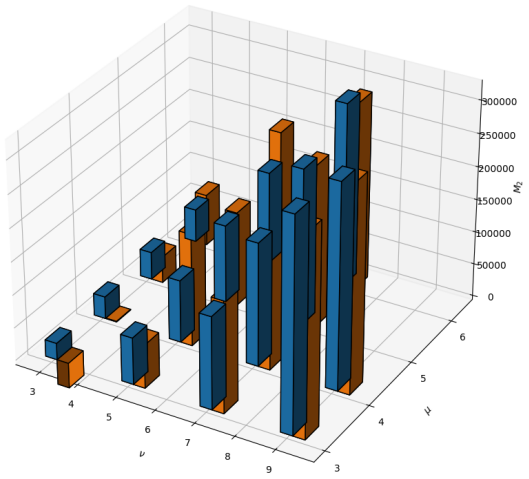

Figure 56. Second Zagreb index vs ν and μ.

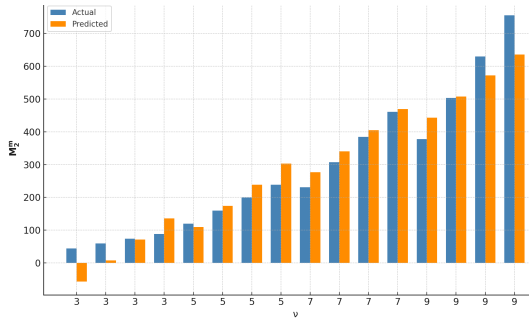

Figure 57. Modified second Zagreb index vs ν.

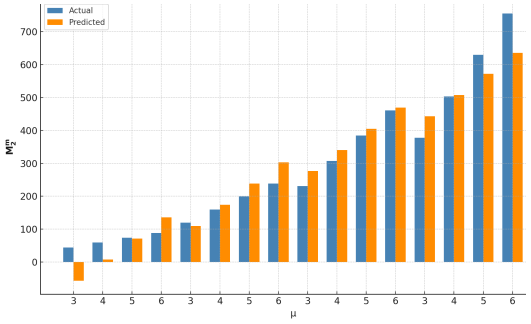

Figure 58. Modified second Zagreb index vs μ.

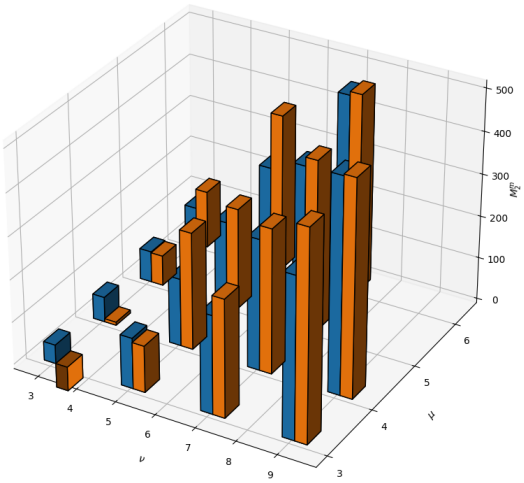

Figure 59. Modified second Zagreb index vs ν and μ.

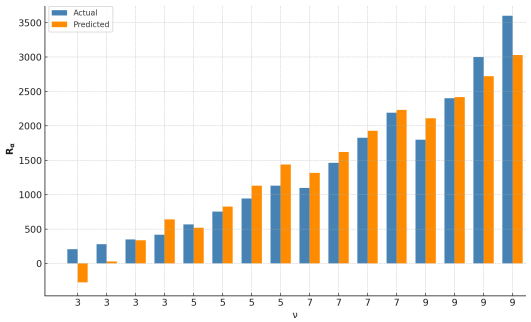

Figure 60. General Randić index vs ν.

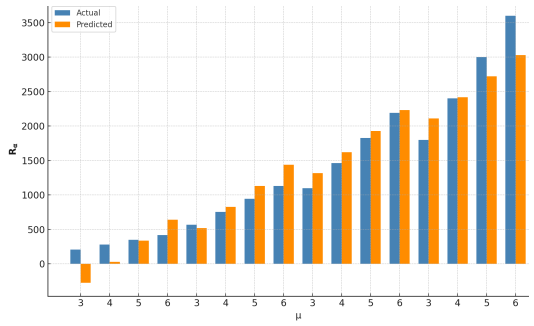

Figure 61. General Randić index vs μ.

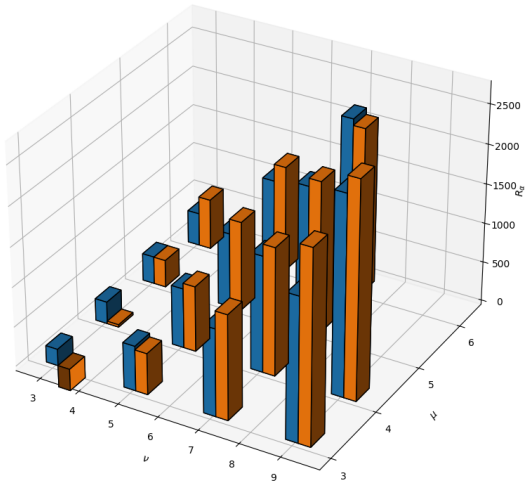

Figure 62. General Randić index vs ν and μ.

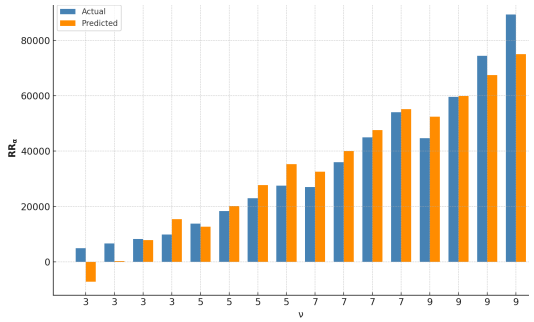

Figure 63. Inverse Randić index vs ν.

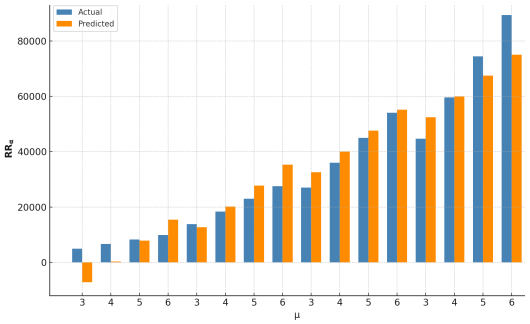

Figure 64. Inverse Randić index vs μ.

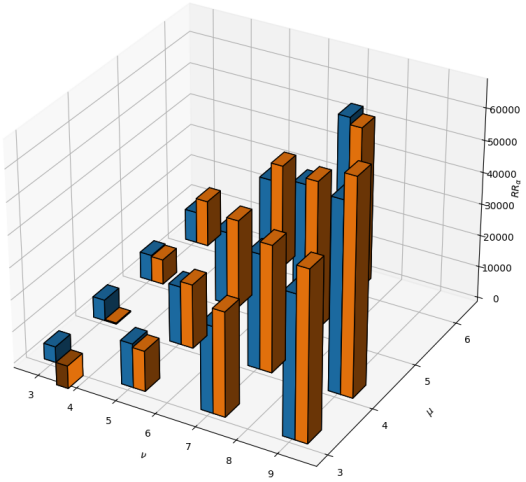

Figure 65. Inverse Randić index vs ν and μ.

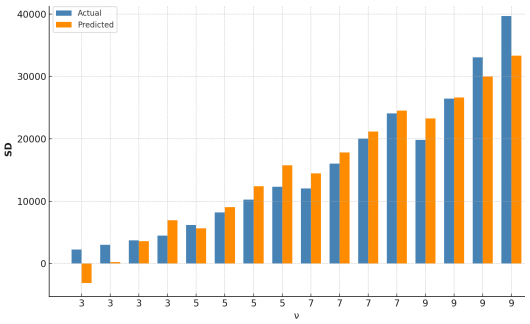

Figure 66. Symmetric division index vs ν.

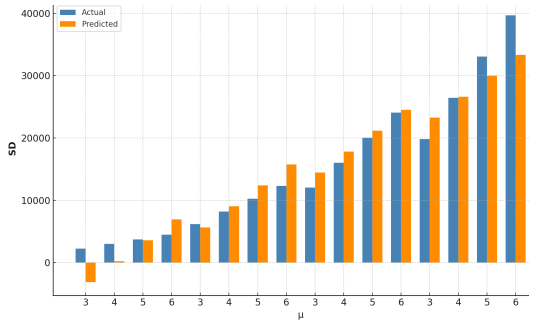

Figure 67. Symmetric division index vs μ.

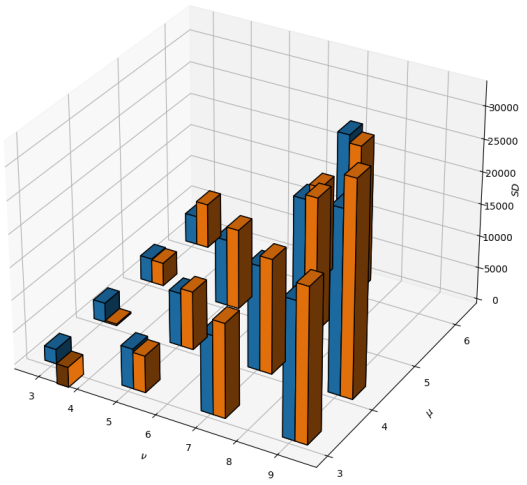

Figure 68. Symmetric division index vs ν and μ.

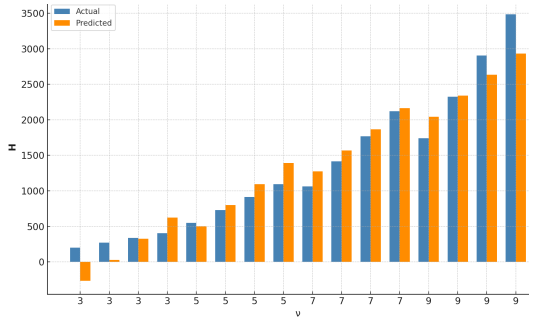

Figure 69. Harmonic index vs ν.

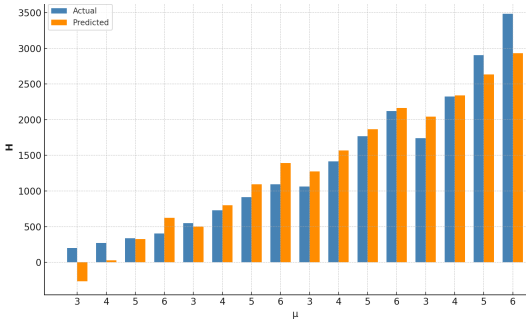

Figure 70. Harmonic index vs μ.

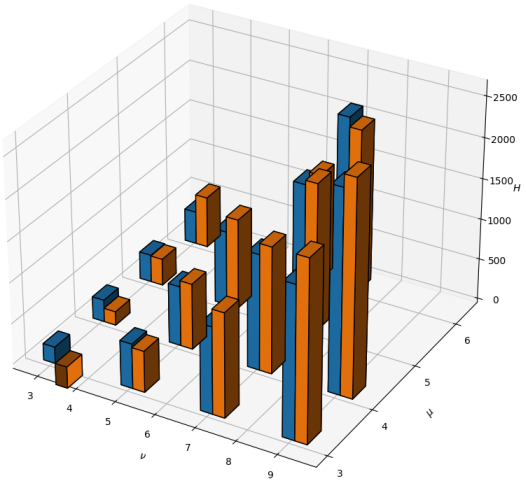

Figure 71. Harmonic index vs ν and μ.

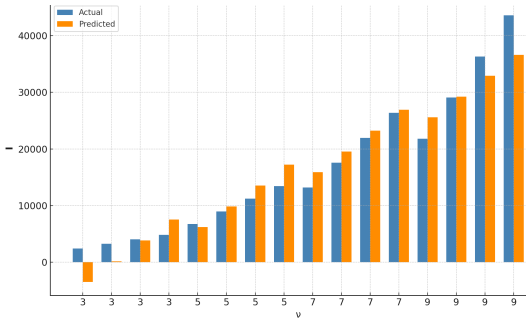

Figure 72. Sum inverse index vs ν.

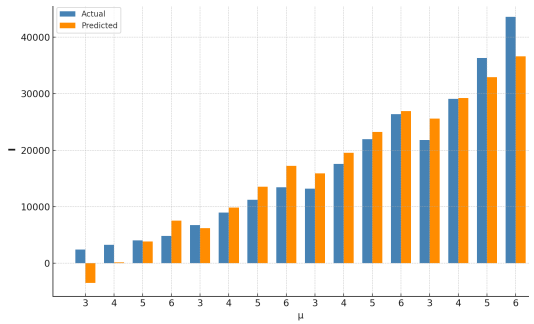

Figure 73. Sum inverse index vs μ.

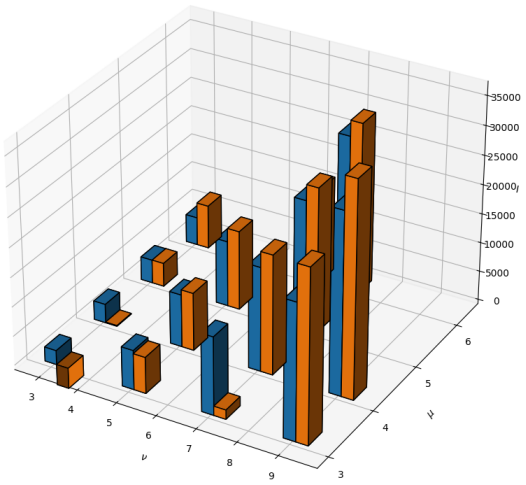

Figure 74. Sum inverse index vs ν and μ.

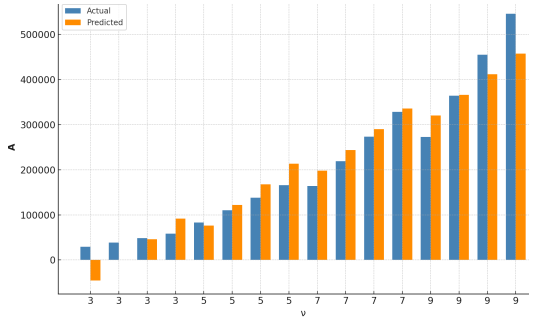

Figure 75. Augmented Zagreb index vs ν.

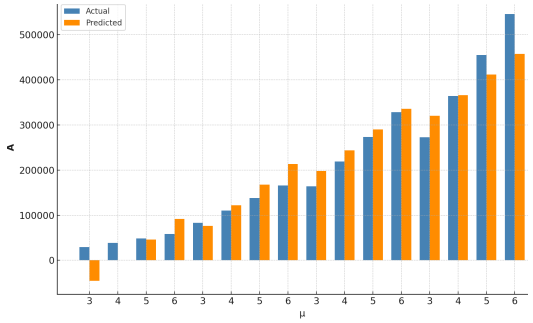

Figure 76. Augmented Zagreb index vs μ.

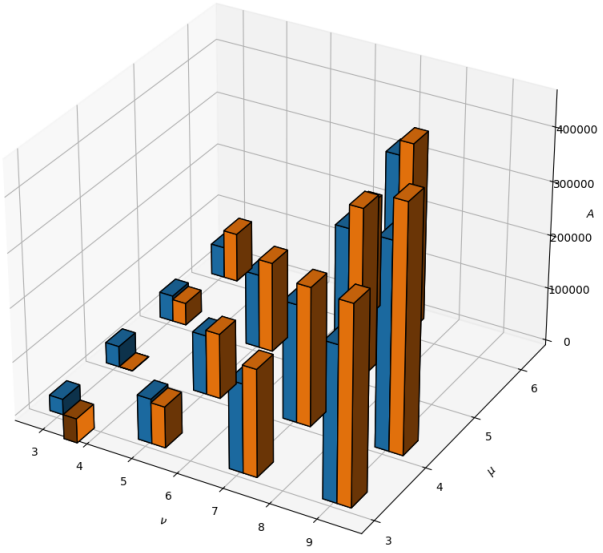

Figure 77. Augmented Zagreb index vs ν and μ.

5.4. Statistical analysis of all indices for when $\nu \geq 3$ is odd and any $\mu \geq 3$

This section presents a statistical analysis of the computed values of nine topological indices of silicate cage molecular networks, specifically $M_1(SLC_\mu(\nu))$, $M_2(SLC_\mu(\nu))$, $M_2^m(SLC_\mu(\nu))$, $R_\alpha(SLC_\mu(\nu))$, $RR_\alpha(SLC_\mu(\nu))$, $SD(SLC_\mu(\nu))$, $H(SLC_\mu(\nu))$, $I(SLC_\mu(\nu))$, and $A(SLC_\mu(\nu))$, evaluated with respect to variations in the number of layers ν and the number of replicated units μ. These indices are visualized using 2D and 3D graphical representations along both parameters. A detailed discussion of the observed trends follows.

With respect to ν: The statistical evaluation shows that all considered topological indices exhibit a consistent increasing trend with respect to the number of layers (ν). This indicates that these indices are strongly influenced by the growth of the silicate cage molecular network. Indices such as M_1, M_2, M_2^m, R_α, and RR_α show systematic variation with increasing ν, reflecting their dependence on degree-based structural properties and connectivity patterns. Similarly, indices such as SD, H, I, and A also increase steadily, indicating sensitivity to the overall structural complexity and network expansion. Overall, the variation with respect to ν demonstrates that these indices effectively capture the size-dependent structural characteristics of the molecular network, making them useful for describing graph-based chemical structures.

With respect to μ: The analysis with respect to the number of replicated units (μ) shows that all indices exhibit a measurable dependence on edge multiplicity and inter-unit connectivity. In particular, indices such as M_1, M_2, and M_2^m show noticeable variation with increasing μ, indicating their sensitivity to changes in the bonding density. The indices R_α and RR_α also reflect structural variation due to changes in the connectivity patterns. Furthermore, indices such as SD, H, I, and A respond to variations in μ, highlighting their ability to capture changes in the global structural arrangement. Overall, the results indicate that μ influences the connectivity and bonding structure of the network, thereby affecting all considered topologies.

6. Comparative analysis of both cases

The comparison of the three computed Tables 4, 6 and 9 is visually presented in Figure 78, which highlights the differences and trends among the results.

The combined line graph presents a comparative analysis of the nine topological indices M_1, M_2, M_2^m, R_α, RR_α, SD, H, I, and A across three structural cases: When $\mu = 2$, when ν is even, and when ν is odd. Among all indices, the augmented Zagreb index exhibits the steepest growth across all scenarios, indicating its strong sensitivity to increasing molecular structure. M_2 consistently follows, showing rapid escalation, particularly in denser graphs. The modified second Zagreb index (M_2^m) shows moderate growth, which is especially prominent in the $\mu = 2$ case. Both Randić indices reflect smoother trends, suggesting structural stability across different configurations. The symmetric division index shows relatively higher values in the odd ν case but remains less dominant in the $\mu = 2$ condition. On the other hand, the M_1, H, and I indices show a consistent but slower increase, marking them as comparatively stable across topological variations. Overall, the graph reveals that $\mu = 2$ configurations exhibit the most rapid escalation in index values, while even and odd ν structures show distinct but balanced progression patterns, highlighting structural complexity and variation.

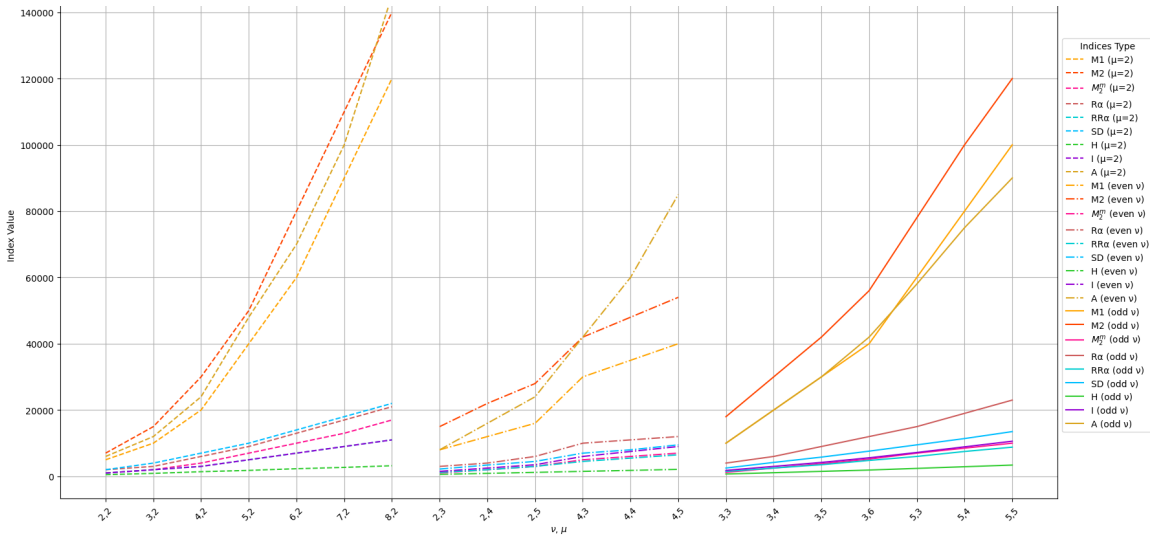

Figure 78. Graphical comparison of topological indices using Tables 4, 7, and 10.

6.1. Structural comparison of all cases

To evaluate the effectiveness of the proposed generalized M-polynomial framework, a comparative assessment is performed against the classical topological index approaches reported in [4, 6, 8]. The comparison focuses on the capacity for structural representation and computational simplicity. The results indicate that the generalized indices provide a more unified symbolic formulation of the considered topological indices. This leads to a reduction in derivation complexity compared with classical methods, making the computation more systematic for large silicate cage networks.

Furthermore, when used in regression-based modeling frameworks, the proposed indices show improved consistency in fitting performance, with a higher coefficient of determination (R^2) compared with traditional index sets. This suggests that degree-weighted extensions capture structural connectivity more effectively. Overall, the proposed framework demonstrates better scalability and capacity for structural representation for complex molecular graph systems, particularly in silicate-based networks.

6.2. Regression-based validation of structural indices

In this study, the computed topological indices of silicate cage molecular networks are further analyzed using regression-based modeling to examine their functional dependence on the structural parameters ν (the number of layers) and μ (the number of replicated units). Since all indices are derived analytically from the underlying graph structure, the purpose of this section is not to perform external machine learning, but to evaluate the consistency and functional stability of the derived expressions through regression fitting. For each topological index, a multivariate polynomial regression model of the form

$$T(\nu, \mu) = a\nu + b\mu + c\nu^2 + d$$

is used to capture the trend behavior and to validate the growth pattern observed in the computed analytical values. The regression coefficients are obtained using least squares fitting over the computed dataset presented in Tables 4, 6, and 9.

The comparison between analytically derived values and regression-fitted curves shows a high degree of agreement, indicating that the proposed indices follow stable and predictable functional relationships with respect to both structural parameters. In most cases, the relationship remains predominantly linear in ν and μ, with minor higher-order contributions appearing in indices that are more sensitive to branching and edge density variations.

Figures 3-77 illustrate the agreement between computed and regression-fitted values for all considered indices, confirming the consistency of the analytical framework.

The regression analysis further highlights that indices such as the augmented Zagreb index $A(\nu, \mu)$ and the second Zagreb index $M_2(\nu, \mu)$ exhibit stronger growth sensitivity compared with other descriptors, making them more suitable for distinguishing structural variations in extended silicate cage networks.

Overall, this regression-based validation confirms that the derived topological indices are not only mathematically consistent but also exhibit stable functional behavior under structural scaling of the parameters ν and μ.

7. Potential applications of silicate cage networks in chemical science

Silicate cage networks, including zeolites, polyhedral oligomeric silsesquioxanes (POSS), and other silica-based frameworks, exhibit high structural regularity, porosity, and chemical tunability. These properties make them highly attractive for a broad spectrum of chemical applications ranging from catalysis and separation to materials design and biomedical technologies. The following are key areas where silicate cage architectures are applied in the field of chemistry and materials science.

- **Heterogeneous catalysis:** Due to their large surface area, acidic sites, and shape-selective channels, silicate cages (especially zeolites) are widely used as solid acid catalysts in petroleum refining, cracking, isomerization, and fine chemical synthesis.
- **Ion-exchange processes:** The negatively charged silicate frameworks can accommodate exchangeable cations (e.g., Na^+, K^+, Ca^{2+}), which enables their use in ion-exchange chromatography, water softening, and environmental remediation.
- **Molecular sieving and gas separation:** The uniform pore sizes of cage networks allow for selective adsorption and diffusion of gas molecules such as CO_2, CH_4, N_2, and H_2, making them ideal materials for gas purification and storage.
- **Drug delivery and bioconjugation:** Functionalized silicate cages, such as mesoporous silica nanoparticles or POSS derivatives, are utilized as biocompatible drug carriers. Their controllable release behavior and surface functionalization enhance drug loading, targeting, and stability.
- **Sensors and analytical platforms:** Modified silicate cages serve as hosts for fluorescent, electrochemical, or colorimetric sensing systems. Their porous matrices support the immobilization of recognition elements for selective detection of analytes such as metal ions, pH, and biomolecules.
- **Photocatalysis and light harvesting:** Silicate cages doped with transition metals or semiconducting species act as efficient photocatalysts for water splitting, dye degradation, and

solar energy conversion due to their stability and high surface accessibility.

- **Polymer nanocomposites:** Silicate cages like POSS are chemically incorporated into polymer matrices to enhance the thermal stability, mechanical strength, flame retardancy, and oxidation resistance of advanced functional materials.
- **Electrochemical and energy storage materials:** Silicate frameworks are used as supports for lithium-ion battery electrodes, supercapacitor components, and electrolyte membranes owing to their ionic conductivity and structural robustness.
- **Chemical separation and chromatography:** Cage-like silicates are used as stationary phases in chromatographic systems for size exclusion, affinity binding, and polarity-based separations.
- **Green chemistry and environmental catalysis:** Silicate networks serve in environmentally benign catalytic systems, including solvent-free reactions, CO_2 capture, and removal of environmental pollutants such as NO_x, SO_x, and heavy metals.
- **Antibacterial and antifungal coatings:** Functionalized silicate cages can incorporate silver, zinc, or copper ions to produce long-lasting antimicrobial surfaces for medical devices, textiles, and food packaging.
- **Controlled release fertilizers:** Silicate cages are used as slow-release matrices for nitrogen, phosphorus, and micronutrients, enhancing crop efficiency and reducing nutrient leaching in precision agriculture.
- **Smart windows and coatings:** Silicate networks embedded with thermochromic or photochromic compounds help regulate light and heat transmission in energy-saving glass technologies.
- **Flame-retardant materials:** POSS and other silicate cages, when integrated into polymers, drastically reduce flammability by forming protective ceramic-like char layers during combustion.
- **Biomedical imaging and theranostics:** Silica nanoparticles are functionalized with contrast agents (e.g., Gd, Au, fluorescent dyes) for magnetic resonance imaging, positron emission tomography, and optical imaging applications, often integrated with therapeutic payloads (theranostics).
- **Nano-encapsulation of flavors and fragrances:** Silicate cages protect volatile compounds in perfumes, detergents, and food additives, enabling long-lasting aroma and controlled release upon use.
- **Proton and ion conductive membranes:** Sulfonated or phosphate-functionalized silicate frameworks serve as ion-conductive phases in proton-exchange membranes for fuel cells and electrochemical sensors.
- **CO_2 capture and climate technology:** Amine-functionalized mesoporous silicates are efficient adsorbents for selective CO_2 capture from flue gases, contributing to carbon reduction strategies.
- **Template-assisted synthesis of nanomaterials:** Silicate cages serve as hard templates for synthesizing nanowires, hollow spheres, and core–shell structures of metals, metal oxides, or carbon materials.
- **Cosmetic enhancers and fillers:** Silica particles enhance the sensory feel, oil control, and sun protection factor (SPF) efficiency in sunscreens, foundations, and anti-aging formulations due to their light-diffusing properties.
- **Nucleic acid and biomolecule delivery:** Cationic silicate cages can condense and deliver DNA, siRNA, and peptides for gene therapy, showing high cellular uptake and low cytotoxicity.

- **Optical and photonic devices:** Periodic silicate-based structures are used to fabricate photonic crystals, waveguides, and refractive index modulators in optical communications.
- **Reinforcement in aerospace and automotive polymers:** POSS nanofillers improve the modulus, dimensional stability, and weather resistance of polymers used in high-performance transport systems.
- **Scaffolds for tissue engineering:** Bioactive silicate frameworks stimulate cell adhesion, proliferation, and osteogenesis, making them suitable for bone regeneration scaffolds and implants.
- **pH and stimulus-responsive systems:** Smart silicate cages are engineered to release their cargo in response to pH, temperature, or redox stimuli, enabling precision in responsive material design.

These versatile applications underscore the importance of silicate cage networks as foundational materials in modern chemical research, offering structural diversity, reactivity, and compatibility with various chemical environments. Their continued development holds significant promise for innovation across chemical engineering, nanotechnology, and sustainable chemistry.

8. Conclusions

The silicate cage network $SLC_\mu(\nu)$ exhibits well-defined structural behavior across varying values of the number of layers (ν) and the number of replicated units (μ). The studied topological indices, including Zagreb indices (M_1, M_2, M_2^m), Randić index (R_α), inverse Randić index (RR_α), symmetric division index, harmonic index, sum inverse index, and augmented Zagreb index (A), provide effective measures for characterizing the structural complexity of the network.

The results indicate that all considered indices show a consistent and monotonic increase with respect to both ν and μ, reflecting the progressive expansion and enhanced connectivity of the silicate cage structure. This behavior confirms that the indices are sensitive to changes in molecular size and structural density.

For fixed $\mu = 2$, a systematic variation in the index values is observed with increasing ν, while configurations with fewer layers exhibit relatively greater structural fluctuation. However, as ν increases, the behavior of the indices becomes more stable and consistent, indicating improved structural regularity in larger networks.

Among all indices, the augmented Zagreb index and sum inverse index show comparatively higher sensitivity to structural expansion, making them particularly effective in distinguishing changes in complex cage-like topologies.

Overall, the results confirm that the silicate cage network $SLC_\mu(\nu)$ provides a scalable and structurally consistent framework for topological analysis. The studied indices effectively capture variations in connectivity and molecular growth, making them suitable for applications in graph-theoretical chemistry and structure-based modeling.

Future extensions of this work may explore similar topological frameworks for other inorganic and hybrid networks, enabling broader applications in molecular modeling and the structural analysis of complex materials.

Authors contributions

Zhang Yan: Validation, visualization, manuscript preparation and improvement, revision of the manuscript, preparation and refinement of figures and graphical illustrations; Muhammad Salman: Supervision and conceptualization; Syed Shahzaib: Investigations, methodology; Imran Khalid: Writing-initial and final drafts; Hanen Karamti: Formal analysis. All the authors have read and approved the final version of the article.

Use of Generative-AI tools declaration

During the preparation of this manuscript, the authors used ChatGPT solely for language editing and improving the clarity, grammar, and readability of the text. The authors carefully reviewed and revised all AI-assisted content and take full responsibility for the accuracy, originality, and integrity of the final manuscript

Acknowledgments

Princess Nourah bint Abdulrahman University Researchers Supporting Project number (PNURSP2026R192), Princess Nourah bint Abdulrahman University, Riyadh, Saudi Arabia.

Conflict of interest

The authors stated that there were no competing interests in connection with the work reported in this article.

References

1. A. T. Balaban, Applications of graph theory in chemistry, *J. Chem. Inf. Comput. Sci.*, **25** (1985), 334–343. https://doi.org/10.1021/ci00047a033
2. G. Wu, M. W. Rasheed, S. Alsulami, SMILES-based degree molecular descriptors and machine learning for QSPR modeling of anti-alkaptonuria drugs, *Front. Chem.*, **14** (2026), 1845927. https://doi.org/10.3389/fchem.2026.1845927
3. H. Hosoya, Topological index. A newly proposed quantity characterizing the topological nature of structural isomers of saturated hydrocarbons, *Bull. Chem. Soc. Jpn.*, **44** (1971), 2332–2339. https://doi.org/10.1246/bcsj.44.2332
4. I. Gutman, N. Trinajstić, Graph theory and molecular orbitals. Total φ-electron energy of alternant hydrocarbons, *Chem. Phys. Lett.*, **17** (1972), 535–538. https://doi.org/10.1016/0009-2614(72)85099-1
5. G. Zhang, S. Noureen, S. Azam, M. E. M. Abdalla, M. E. Dafaalla, A. Aslam, et al., Leveraging topological indices and machine learning for advanced prediction of antidepressant drug properties, *Sci. Rep.*, **16** (2026), 3537. https://doi.org/10.1038/s41598-025-33532-3

6. M. Randić, Characterization of molecular branching, *J. Am. Chem. Soc.*, **97** (1975), 6609–6615. https://doi.org/10.1021/ja00856a001
7. P. Schwaller, A. C. Vaucher, R. Laplaza, C. Bunne, A. Krause, C. Corminboeuf, et al., Machine intelligence for chemical reaction space, *Wiley Interdiscip. Rev.: Comput. Mol. Sci.*, **12** (2022), e1604. https://doi.org/10.1002/wcms.1604
8. E. Deutsch, S. Klavžar, M-polynomial and degree-based topological indices, *Iran. J. Math. Chem.*, **6** (2015), 93–102. https://doi.org/10.22052/IJMC.2015.10106
9. W. E. Ahmed, M. Naeem, M. K. Siddiqui, M. A. Fiidow, Predictive modeling of ADME properties using M-polynomial based topological indices for biocompatible polysaccharides, *Sci. Rep.*, **15** (2025), 29667. https://doi.org/10.1038/s41598-025-14134-5
10. M. C. Day, F. C. Hawthorne, Bond topology of chain, ribbon and tube silicates. Part I. Graph-theory generation of infinite one-dimensional arrangements of $(TO_4)^{n-}$ tetrahedra, *Found. Crystallogr.*, **78** (2022), 212–233. https://doi.org/10.1107/S2053273322001747
11. R. Abdusalamov, C. Scherdel, M. Itskov, B. Milow, G. Reichenauer, A. Rege, Modeling and simulation of the aggregation and the structural and mechanical properties of silica aerogels, *J. Phys. Chem. B*, **125** (2021), 1944–1950. https://doi.org/10.1021/acs.jpcb.0c10311
12. S. Mohankumar, P. Sivakumar, S. Priyatharshni, Graph-theoretic and computational analysis of QSAR molecular descriptors for single chain diamond silicates, *Discov. Chem.*, **2** (2025), 108. https://doi.org/10.1007/s44371-025-00186-z
13. A. L. Samuel, Some studies in machine learning using the game of checkers, *IBM J. Res. Dev.*, **3** (1959), 210–229. https://doi.org/10.1147/rd.33.0210
14. Y. LeCun, Y. Bengio, G. Hinton, Deep learning, *Nature*, **521** (2015), 436–444. https://doi.org/10.1038/nature14539
15. V. N. Vapnik, *The nature of statistical learning theory*, Springer New York, 1995. https://doi.org/10.1007/978-1-4757-2440-0
16. Y. T. Shih, Y. Shi, L. Huang, Predicting glass properties by using physics-and chemistry-informed machine learning models, *J. Non-Cryst. Solids*, **584** (2022), 121511. https://doi.org/10.1016/j.jnoncrysol.2022.121511
17. J. B. Liu, K. Wang, X. Zhai, Statistical analysis and topological property of a class of fractal networks, *Fractals*, **34** (2026), 2640001. https://doi.org/10.1142/S0218348X26400013
18. S. Mondal, M. K. Siddiqui, N. De, A. Pal, Neighborhood M-polynomial of crystallographic structures, *Biointerface Res. Appl. Chem*, **11** (2021), 9372–9381. https://doi.org/10.33263/BRIAC112.93729381
19. Y. Chen, X. Liu, M. Deveci, Z. Wang, S. Zhang, Preference disaggregation-based multiclass Mahalanobis-Taguchi system applied to medical insurance fraud, *Eng. Appl. Artif. Intel.*, **167** (2026), 113934. https://doi.org/10.1016/j.engappai.2026.113934
20. M. Javaid, J. Cao, Computing topological indices of probabilistic neural network, *Neural Comput. Appl.*, **30** (2018), 3869–3876. https://doi.org/10.1007/s00521-017-2972-1

21. M. U. Ghani, S. Ali, M. Imran, H. Karamti, F. Sultan, M. Y. Almusawa, Hex-derived molecular descriptors via generalized valency-based entropies, *IEEE Access*, **11** (2023), 42052–42068. https://doi.org/10.1109/ACCESS.2023.3248507

22. A. Ilić, D. Stevanović, On comparing Zagreb indices, *arXiv*, 2011. https://doi.org/10.48550/arXiv.1104.4262

23. B. Liu, I. Gutman, On general Randic indices, *MATCH Commun. Math. Comput. Chem.*, **58** (2007), 147–154.

24. J. B. Liu, F. Zou, G. J. Cai, J. Cao, Network coherence and robustness analysis of extended polygonal networks, *Circuits Syst. Signal Process.*, 2026. https://doi.org/10.1007/s00034-026-03526-1

25. J. B. Liu, M. Y. Yu, G. J. Cai, J. Cao, The leader–follower coherence and spectral properties of weighted recursive networks under noise disturbance, *Chaos Soliton. Fract.*, **208** (2026), 118060. https://doi.org/10.1016/j.chaos.2026.118060

26. S. Fajtlowicz, On conjectures of Graffiti, *Ann. Discrete Math.*, **38** (1988), 113–118. https://doi.org/10.1016/S0167-5060(08)70776-3

27. L. Zhong, The harmonic index for graphs, *Appl. Math. Lett.*, **25** (2012), 561–566. https://doi.org/10.1016/j.aml.2011.09.059

28. J. Sedlar, D. Stevanović, A. Vasilyev, On the inverse sum indeg index, *Discrete Appl. Math.*, **184** (2015), 202–212. https://doi.org/10.1016/j.dam.2014.11.013

29. B. Furtula, A. Graovac, D. Vukičević, Augmented Zagreb index, *J. Math. Chem.*, **48** (2010), 370–380. https://doi.org/10.1007/s10910-010-9677-3

AIMS Press